Seasonal and interannual variability of the Subtropical Front in the New Zealand region

Erik Behrens[1], Andrew McC. Hogg[2], Matthew H. England[3], and Helen Bostock[4]

[1]NIWA
[2]Australian National University
[3]University of New South Wales
[4]University of Queensland

November 21, 2022

Abstract

The meridional variability of the Subtropical Front (STF) and the drivers of variability on interannual time scales in the New Zealand region are analysed using a multi-decadal eddy-resolving ocean hindcast model, in comparison with Argo data. The STF marks the water mass boundary between subtropical waters and subantarctic waters, and is defined as the southern-most location of the 11 degree C isotherm and 34.8 isohaline between 100 m and 500 m. The STF shifts up to 650 km (6 degree) meridionally on seasonal timescales. In addition to seasonal variability, shifts of around 200 km (2 degree) occur on interannual time scales. These shifts are connected to local wind stress curl anomalies in the eastern Tasman Sea, which trigger Ekman convergence/divergence and result in meridional transport of heat and salt into/out of the Tasman Sea. The net transports across the northern boundary of the Tasman Sea show the largest sensitivity to these wind stress curl anomalies. During periods of positive wind stress curl anomalies and Ekman convergence, the heat and salt content increases shifting the position of the STF southward. The opposite tendency occurs during periods of negative wind stress curl anomalies. The migration of the STF does not appear to be directly linked to regional climate oscillations.

Seasonal and interannual variability of the Subtropical Front in the New Zealand region

Erik Behrens[1], Andrew McC. Hogg[2], Matthew H. England[3], Helen Bostock[4]

[1] National Institute of Water and Atmospheric Research, Wellington, New Zealand

[2] Research School of Earth Science and ARC Centre of Excellence for Climate Extremes, The Australian National University, Canberra, Australia

[3] Climate Change Research Centre and ARC Centre of Excellence for Climate Extremes, University of New South Wales, Sydney, Australia

[4] The University of Queensland, Brisbane, Australia

Corresponding author: Erik Behrens, erik.behrens@niwa.co.nz

Key points:

- The location of the Subtropical Front varies on seasonal to decadal time scales with larger meridional shifts away from shallow bathymetry
- Over the Tasman Sea interannual variability is connected to upper ocean heat and freshwater content anomalies, driven by oceanic transports
- These anomalous transports are a consequence of local wind stress curl anomalies in the eastern Tasman Sea

Abstract

The meridional variability of the Subtropical Front (STF) and the drivers of variability on interannual time scales in the New Zealand region are analysed using a multi-decadal eddy-resolving ocean hindcast model, in comparison with Argo data. The STF marks the water mass boundary between subtropical waters and subantarctic waters, and is defined as the southern-most location of the 11°C isotherm and 34.8 isohaline between 100 m and 500 m. The STF shifts up to 650 km (6°) meridionally on seasonal timescales. In addition to seasonal variability, shifts of around 200 km (2°) occur on interannual time scales. These shifts are connected to local wind stress curl anomalies in the eastern Tasman Sea, which trigger Ekman convergence/divergence and result in meridional transport of heat and salt into/out of the Tasman Sea. The net transports across the northern boundary of the Tasman Sea show the largest sensitivity to these wind stress curl anomalies. During periods of positive wind stress curl anomalies and Ekman convergence, the heat and salt content increases shifting the position of the STF southward. The opposite tendency occurs during periods of negative wind stress curl anomalies. The migration of the STF does not appear to be directly linked to regional climate oscillations.

Plain language summary:

In this paper we investigate how the Subtropical Front around New Zealand varies in space and time. The Subtropical Front is a water mass boundary between subtropical and subantarctic waters and is a region of high biological production due to favourable oceanic conditions (e.g. nutrients and temperature). We observe large seasonal shifts of around 650 km in the open ocean, while reduced near the coast. During summertime the Subtropical Front is located further south than during winter. In addition to the seasonal shifts, interannual variability in the order of 200km is observed too. Large part of this long-term variability can be linked to heat and salinity changes within the Tasman Sea, mainly driven by changes in local wind pattern in the eastern Tasman Sea.

1. Introduction

The Subtropical Front (STF) defines the boundary between warm, salty subtropical waters and the cold, fresh and subantarctic water masses of the Southern Ocean (Deacon 1982; Orsi, Whitworth, and Nowlin 1995; Belkin and Gordon 1996; Sokolov and Rintoul 2009a). Due to the different water mass properties of the subtropical water and subantarctic water, large differences across the STF of about 4-5°C in temperature and 1 psu in salinity occur over distances of ~200 km (Deacon 1982; Belkin and Gordon 1996). In some regions the STF is wider, but still characterised by temperature gradients >1°C/100 km (Smith et al. 2013). The mean position of the STF is around 40°S (Hamilton 2006), but large meridional variations of ±10° occur along its path around the Southern Hemisphere, also depending on the definition of the STF. The mean meridional location of the STF defies oceanographic theories, which suggest that the position the STF should be located at the latitude of zero wind stress curl at around 50°S (De Boer et al. 2013). This mismatch between theory and observations has drawn the attention of several modelling studies to improve our understanding about the position of the STF globally, and how it may respond to future climate change (Graham et al. 2012; De Boer et al. 2013). However, these climate change studies have used relatively coarse (1°×1°) ocean models e.g. (Graham et al. 2012; Meijers 2014), which do not resolve mesoscale processes.

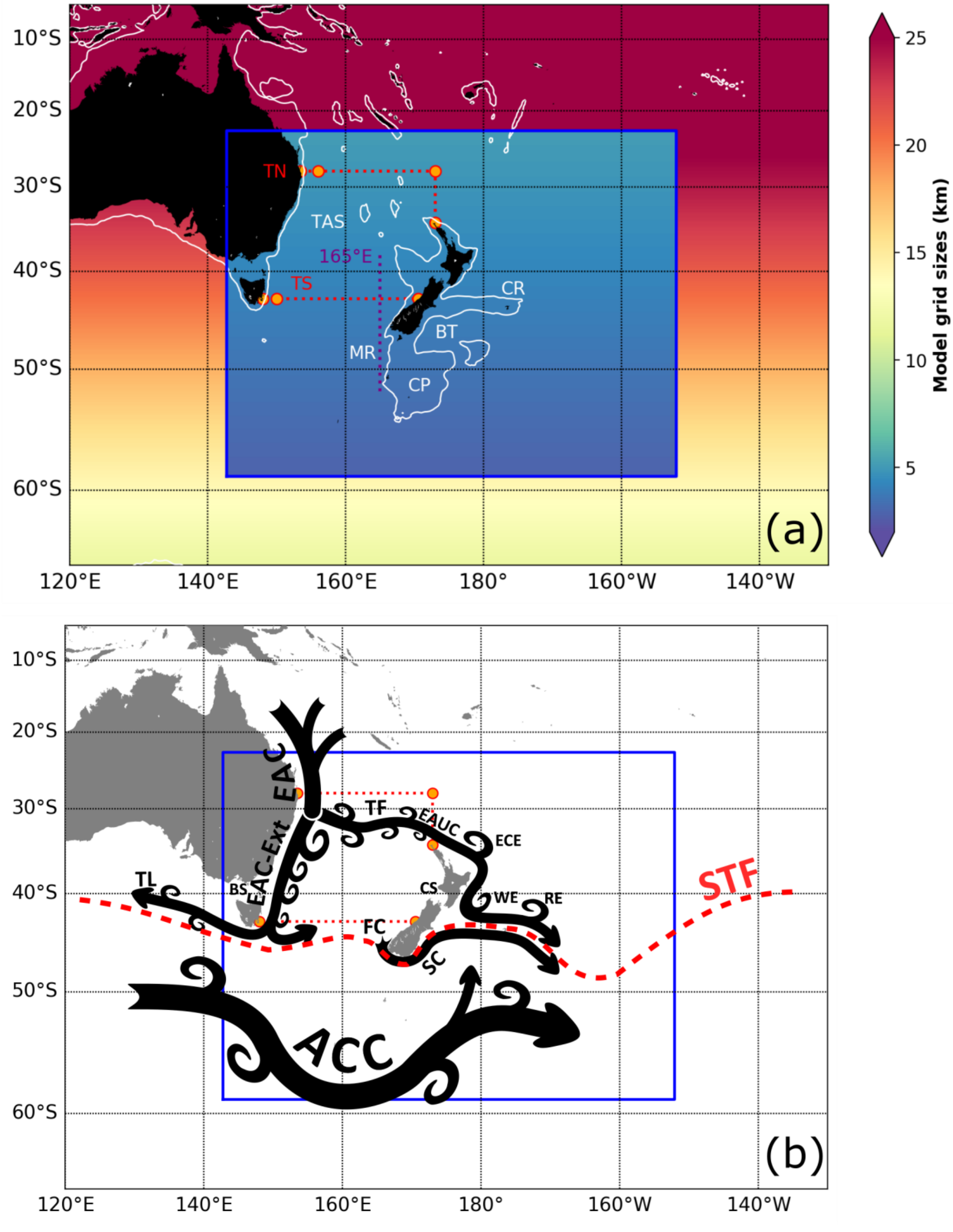

Figure 1a. Model grid sizes of the NZ20 configuration in km as colour shading. White contour line shows the 1000m iso-bath. Two sections have been defined to enclose the majority of the Tasman Sea (red dotted), the Tasman North (TN) and Tasman South (TS) section. The orange dots along the sections mark the segments which have been used to calculate transports. A meridional section at 165°E (purple dotted line) has been defined to illustrate the temperature and salinity structure over the water column in the STF region. The Macquarie Ridge (MR), Campbell Plateau (CP), Chatham Rise (CR), Bounty Through (BT), and Tasman Sea (TAS) have been labelled. (b) Schematic of major ocean

currents in the region: East Australian Current (EAC), East Australian Current Extension (EAC-Ext), Tasman Front (TF), East Auckland Current (EAUC), Fiordland Current (FC), Southland Current (SC), Antarctic Circumpolar Current (ACC). The Bass Strait (BS), Cook Strait (CS), East Cape Eddy (ECE), Wairarapa Eddy (WE) and Rekohu Eddy (RE) have been labelled. The location of the Subtropical Front (STF) has been indicated by the dashed red line.

In this paper we compare the position of the STF on seasonal to interannual scales around New Zealand using Argo hydrographic data and a new high-resolution, eddy-resolving, ocean model for the New Zealand region and South West (SW) Pacific. This resolution is important as the ocean around New Zealand, including the STF region, is dominated by mesoscale eddies on various spatial and temporal scales (Oliver, O'Kane, and Holbrook 2015; Bull et al. 2017; Oke, Pilo, et al. 2019). Thus, high-resolution ocean models, that can fully resolve the mesoscale processes, are critical to understanding the dominant processes and variability of the STF in this region.

The paper is organised as follows. Section 1.1 and 1.2 summarise the previous issues with defining the STF and give an introduction into the regional oceanography of the SW Pacific. Section 2 describes the models which we use for this study, lays out the STF tracking algorithm and introduces the methods (e.g. section and regions) to investigate changes in the location of the STF. Section 3 contains the model validation. Section 4.1 presents the mean location of the STF, and section 4.2/4.3 the seasonal/interannual variability of the STF. Section 4.4 links the interannual variability of the STF in the Tasman Sea to meridional transport and local wind stress curl. Section 5 provides a discussion and conclusion.

1.1 Definitions of the STF

Previously, the STF has been defined by temperature and salinity criteria and/or their gradient depending on the specific focus and dataset used in the study (Belkin and Gordon 1996; Graham and De Boer 2013; Orsi, Whitworth, and Nowlin 1995). Depending on the definition of the STF, this has led to multiple distinct fronts (e.g. Northern STF and Southern STF) being identified at one longitude in the SW Pacific (Belkin and Gordon 1996; Burls and Reason 2006; Sutton and Roemmich 2001; Kostianoy et al. 2004; Hamilton 2006). In regions away from bathymetry, it has been noted that the STF consists of a band of fronts, which is referred to as Subtropical Frontal Zone (STFZ), where the Northern and Southern STF mark its boundary. It has also been found that properties along the STF path evolve and change due to cross-frontal processes and interaction with the bathymetry (Graham et al. 2012). Unlike the Subantarctic Front (SAF) and Antarctic Polar Front, it is not possible to define the STF based on sea surface height (SSH) as the STF is density compensated and shows only relative weak flows in some regions (Sokolov and Rintoul 2002; Smith et al. 2013). A range of dynamical approaches have been developed to define the STF as the southern boundary between the subtropical Super Gyre and the Antarctic Circumpolar Current (ACC) (Smythe-Wright et al. 1998; Stramma 1992). The Super Gyre connects all three subtropical gyres in the Southern Hemisphere (Cai 2006). These studies aimed to link the STF directly to ocean dynamics, and have led to definitions of a dynamical STF, associated with the western boundary currents of the subtropical gyres (Graham and De Boer 2013).

1.2 Regional oceanography around New Zealand

The New Zealand land mass, and associated bathymetry of the continent of Zealandia (Mitchell et al. 2012; Seton et al. 2017) sits at the boundary between the subtropical water in the South Pacific subtropical gyre, and the subantarctic water in the Southern Ocean (Chiswell et al., 2015). This complex bathymetry has a strong influence on the position of the STF (Sutton, 2001; Uddstrom and Oien 1999) and other fronts and currents in this region such as the SAF and ACC (Morris et al., 2001; Sokolov and Rintoul, 2009; Chiswell et al., 2015). Previous work around New Zealand has used hydrographic and satellite data to define the position and the properties of the STF (Edwards and Emery 1982; Jeffrey 1986; Butler et al. 1992; Szymanska and Tomczak 1994; Uddstrom and Oien 1999; Morris, Stanton, and Neil 2001; Belkin and Cornillon 2003; Hamilton 2006; Smith et al. 2013). Some of these studies have suffered from distinguishing between local neritic fronts and issues with shallow bathymetry, placing the position of the STF in a wide range of locations, especially in the Tasman Sea and south of New Zealand (Belkin and Cornillon 2003; Hamilton 2006; Smith et al. 2013). Local hydrographic observations have also been used to investigate the fine scale structure and variability of the STF, both in the Tasman Sea and east of New Zealand (Sutton 2001; Chiswell 2001, 2002; Smith et al. 2013). They revealed that the STF can be separated into a northern and southern front. Low and medium resolution modelling studies have previously been used to investigate the response of the STF to changes in wind stress curl and the complex bottom topography in this region (Tilburg et al. 2002). They found that the STF east of New Zealand is controlled by topography and by westward propagating surface layer thickness gradients.

2. Methods

2.1 Model description

This modelling study is based on output from two forced ocean - sea-ice models, which use NEMO and CICE to simulate the ocean circulation and sea-ice physics respectively. A detailed description of the model setup, known as GO6, can be found in (Storkey et al. 2018). The first model for our study uses the global ¼° horizontal eORCA grid of ~20 km, hereafter eORCA025. eORCA025 is partially mesoscale resolving, also known as eddy-permitting. The second model is identical to eORCA025, but has a high-resolution (1/20°) nested region embedded around New Zealand (Figure 1), in which the grid length is around 4 km, hereafter called NZ20, In this nested region, the model fully resolves mesoscale processes (and partially resolves sub-mesoscale dynamics). The two-way nesting between the global and high-resolution domain is accomplished by AGRIF (Debreu, Vouland, and Blayo 2008). The high-resolution domain of NZ20 stretches from 142.8°E to 152°W and 59°S to 22°S, with 1304 and 1004 grid cells in x and y direction. Both models use 75-vertical z-levels in combination with a partial cell approach (Barnier et al. 2006). Layer thickness varies between 1 m at the surface and 200 m in the deep ocean.

In both models a hindcast simulation from 1958-2018 has been performed with atmospheric reanalysis conditions based on JRA-55-DO v1.3 (Tsujino et al. 2018). The simulations have been started from rest with temperature and salinity fields based on an EN4 climatology (Good, Martin, and Rayner 2013). A coastal runoff climatology has been applied, and sea surface salinity has been restored to the EN4 climatology with time scales of 30 days for the 1 m depth surface layer. Due to the cold start of both simulations, timeseries in this paper are presented from 1980 onward to allow for potential spin-up effects. Model data has been stored as 5 day means over the simulation period, but the bulk of diagnostics for this paper have been performed using monthly means.

The model output is compared with the Roemmich-Gilson Argo climatology (Roemmich and Gilson 2009), hereafter referred to as Argo, which provides monthly means for temperature and salinity on a 1° grid. SSH data of absolute dynamic topography from satellite has also been used, which is based on a multi-mission altimeter product (Ssalta/Duacs) from Archiving, Validation and Interpretation of Satellite Oceanography data (hereafter referred to as AVISO).

2.2 Definition of the STF

In this study we adopted the STF definition of Orsi et al. (1995) with fixed thresholds for temperature (11°C, STF_{TEMP}) and salinity (34.8 psu, STF_{SALT}) and their southernmost location between 100 m and 500 m to identify the STF. The depth range is a slight variation of Orsi et al. (1995), who used the temperature and salinity values at 100 m water depth. This variation was motivated by the subsurface salinity maximum of subtropical waters, which is located deeper than 100 m in some regions due to changes in the mixed layer depth, resulting in minor regional differences between both approaches. Overall, using fixed water mass values below the surface reduces the seasonal variability in the STF (Orsi, Whitworth, and Nowlin 1995). The STF based on temperature and salinity is hereafter STF_{TEMP} and STF_{SALT}.

To aid the comparison between data sources with different spatial scales, we apply the most generic and robust criteria (fixed discrete values) to track the STF. We note that the location of the STF depends highly on the selected values for temperature and salinity. Warmer and saltier values will result in a more northerly location of the STF, while cooler and fresher values will yield a more southward position of the STF. Following previous studies, the sensitivity to our choices has been tested by considering variations of ±1°C and ±0.2 psu around our selected values to provide a measure of uncertainty (Orsi, Whitworth, and Nowlin 1995). Results show a meridional shift of between 107 km to 278 km for NZ20 (95 km to 277 km for Argo) per 1°C and 56km to 738 km (1 km to 1420 km) per 0.2 psu over the region from 1980 to present. The regions with the largest shifts are in the open ocean, with less variation near the coast.

2.3 Control cross sections and regions

We used two control sections to evaluate modelled temperature, salinity and cross section velocity and transports. These control sections enclose a large part of the Tasman Sea (Figure 1; Table 1). The Tasman North section at 28°S, cuts through the East Australian Current (EAC) before the current bifurcates at ~32°S into an eastward flow along the Tasman Front and southward flow as part of the EAC Extension (Oliver and Holbrook 2014). This section allows us to quantify volume transports of EAC and Tasman Front and compare them with previous studies. The Tasman South section at 43°S, runs from Tasmania to the West Coast of New Zealand and characterises the Tasman Outflow/Tasman Leakage and the net transport through the Tasman Sea. Both sections enclose the central Tasman Sea (labelled TAS) and only neglect the small transports through the Cook Strait (0.7 Sv) and Bass Strait (0.5 Sv). Transports through these shallow passages with water depths less than 300 m and 155 m, respectively, are considered too minor to affect large scale variability in the central Tasman Sea. The net transport of heat and freshwater across Tasman North and South sections have been used to compute heat and freshwater convergence/divergence and compare them to actual modelled changes, which allows an assessment of the importance of oceanic transports compared to surface fluxes. To compute freshwater a reference salinity of 34.8 psu has been used. In addition to these sections a meridional section along 165°E (marked in Figure 1a and 4), has been used to evaluate temperature and salinity, and to illustrate the location of the STF. Furthermore, two sub-regions in the Tasman Sea (147°E-173°E, 43°S-31°S and 160°E-173°E, 43°-35°S) have also been used to calculate area averages and show the temporal variability of SSH, sea surface temperature (SST) and wind stress curl.

Name	Longitudes	Latitudes
Tasman North (TN)	153.5°E, 156°E, 173°E, 173°E	28°S,28°S, 28°S, 34.4°S
Tasman South (TS)	148°E, 150°E, 170.5°E	43°S, 43°S, 43°S
Tasman Sea (TAS)	148°E, 173°E	28°S, 43°S
165°E	165°E	52°S, 38°S

Table 1. Geographic coordinates for the defined control cross sections and regions shown in Figure 1.

3 Model evaluation

3.1 Mean SSH and SSH variance

Mean SSH fields for AVISO, eORCA025 and NZ20 are shown in Figure 2 a-c to characterise the near surface circulation around New Zealand and evaluate how the models capture the observations. The SSH pattern from all sources shows a meridional gradient between subtropical water and subantarctic water, with higher SSH in the subtropics. Tight contour lines south of 50°S show the influence of the strong ACC. The higher SSH, compared to the broad zonal mean, along the east coast of Australia highlights the EAC and its extension, which is the western boundary current of the South Pacific. On the east coast of the North Island of New Zealand, elevated SSH indicates the East Auckland Current, also part of the western boundary current, and the permanent East Cape Eddy, Wairarapa Eddy and Rekohu Eddy (see also Figure 1b). The SSH contours associated with the SAF and ACC are displaced south by the Campbell Plateau. East of the Campbell Plateau the contours overshoot to the north into the Bounty Trough, before converging at around a latitude of 52°S.

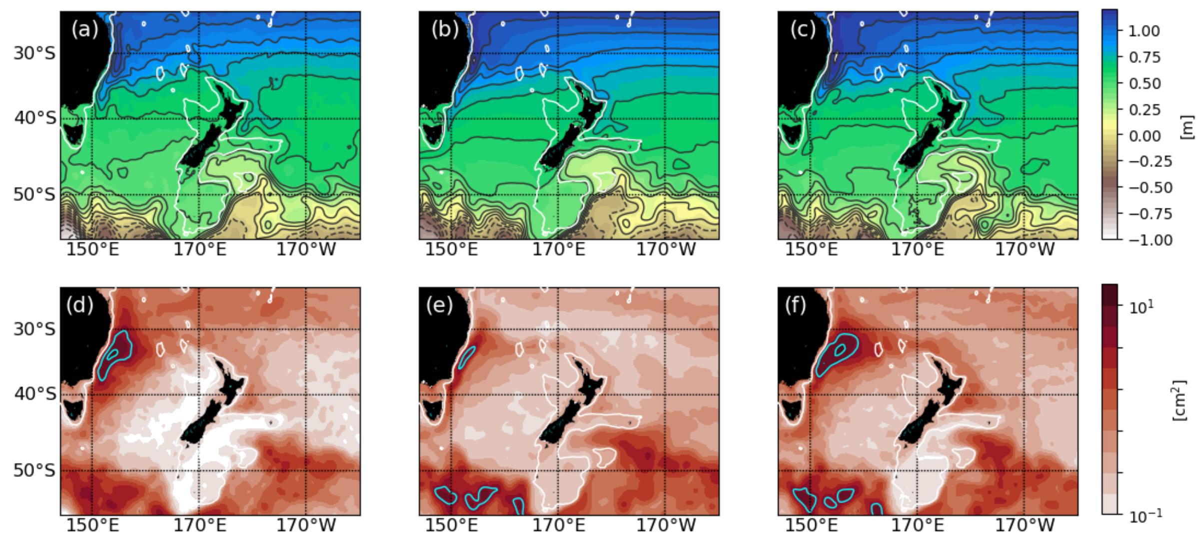

Figure 2. (a-c) Time mean SSH from AVISO, eORCA025 and NZ20 in meter for the period from 1993 to 2018. (d-f) SSH variance for AVISO, eORCA025 and NZ20 in cm^2. Contour interval is 10 cm in (a-c) and 5cm^2 in (d-f).

Both models show good agreement with the observed SSH pattern. Therefore, we argue that the models adequately capture the near-surface oceanic circulation. Comparing the contours over the EAC Extension, Tasman Sea and Tasman Front we see a better match between NZ20 and AVISO than between eORCA025 and AVISO. In eORCA025 the EAC Extension reaches too far south (seen by the higher SSH along the Australian coast), implying an overestimated EAC Extension transport and a weaker zonal flow across the Tasman Sea compared with the AVISO pattern.

To characterise the oceanic eddy field, we compute the SSH variance (Figure 2 d-f) from five-daily averages, which provides an indirect measure for eddy kinetic energy. AVISO shows high variability along the east coast of Australia as part of the EAC and EAC Extension system (Oke, Roughan, et al. 2019). The highest variability is seen south of the EAC bifurcation region, where values reach 10 cm^2. The eddy variability quickly decays with distance away from the coast, with the exception of the Tasman Front as it flows east, which is made up of a series of semi-permanent eddies caused by the interaction of the flow with the north-south bathymetry (Oke, Pilo, et al. 2019). eORCA025 underestimates the eddy activity in both regions due to the coarser model mesh compared to NZ20. Both models, however, capture the variability within the ACC with strong similarities to the observed pattern of eddy variability.

3.2 Mean temperature and salinity properties over the Tasman Sea

In the following we compare the mean temperature and salinity profile over the Tasman Sea for both models against Argo (Figure 3). This diagnostic helps to identify model biases, which influence our STF detection based on temperature and salinity values. The STF is located south of this region, but model biases in this region in combination with ocean advection will impact the STF detection and hence the location of the STF. For example, when negative salinity anomalies, as a consequence of a fresh salinity bias, are advected by oceanic currents southward then the STF detection would place the STF erroneously further north. In addition, this region will also be used to evaluate freshwater and heat content changes, presented in Section 4.4.

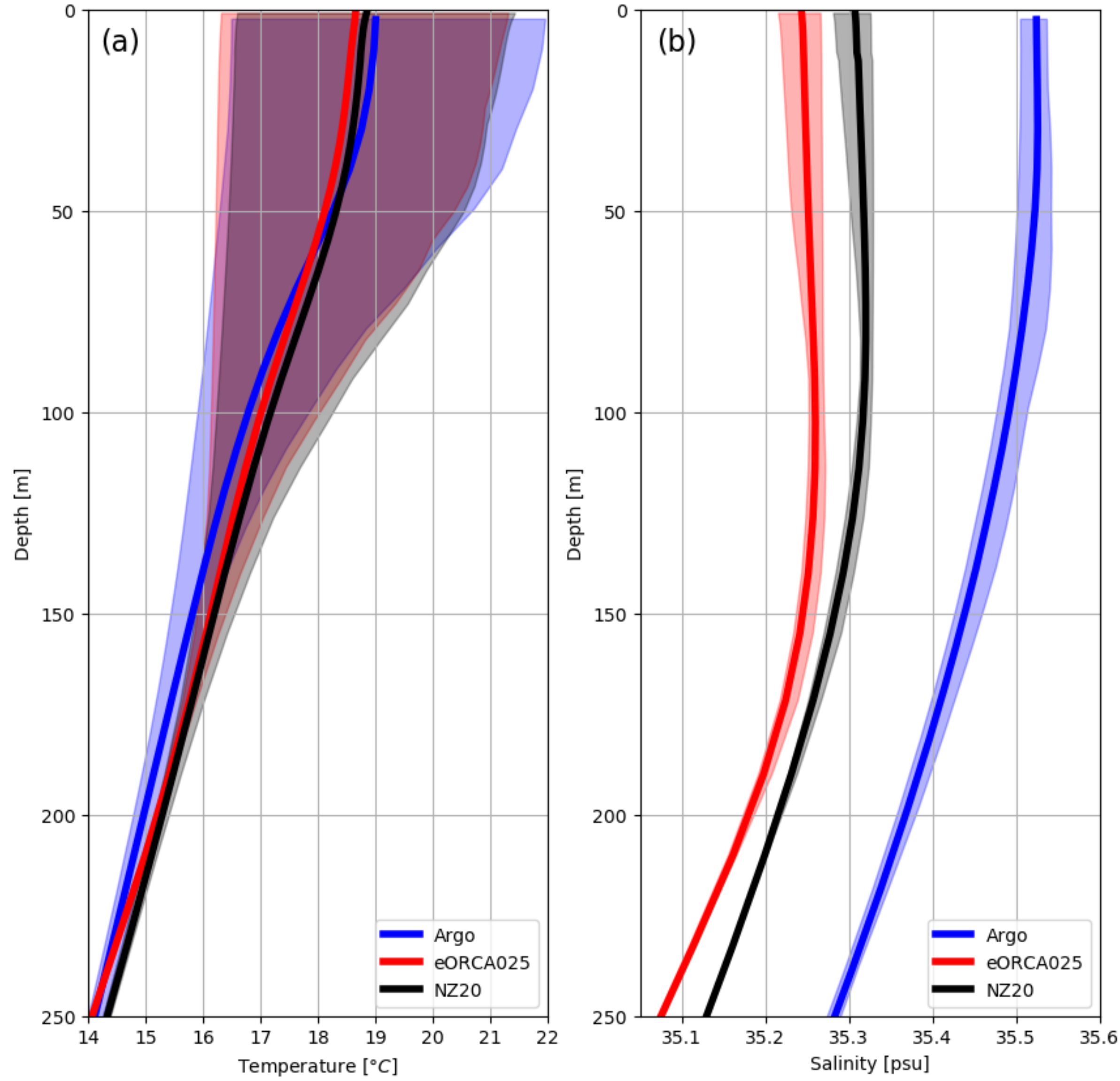

Figure 3: Time averaged temperature (a) and salinity (b) profile over the Tasman Sea are presented as solid lines for Argo, eORCA025 and NZ20 for the period from 2004 to 2018. The range is shown by the colour shading.

The modelled temperature profile for the upper 250 m agrees well with Argo temperature data. Both the mean temperature and the overall range over the water column is well represented in the models. However, both models are up to 0.5°C (eORCA025) / 0.2°C (NZ20) too cold in the upper 50 m and underestimate the upper limit of the range by around 0.7°C. At depth the difference between eORCA025, NZ20 and Argo temperatures are smaller.

Both models underestimate the salinity compared with Argo salinity data. Here, eORCA025 is around 0.3 psu too fresh, while the bias in NZ20 is reduced to 0.2 psu. The Argo profiles show a monotonic freshening with depth, while both models present a local salinity maximum between 70 m and 150 m. Despite this general fresh bias, the modelled salinity range is generally comparable to Argo.

3.3 Upper 200 m model biases

In this section we investigate the spatial pattern of the average temperature and salinity biases from the models compared with Argo data for the surface 200 m (Figure 4). eORCA025 exhibits a large (>1°C) warm bias along the entire east coast of Australia. This bias can be attributed to the EAC Extension, which is too stable in eORCA025 carrying too much heat southward, rather than transporting this heat into the central Tasman Sea. The consequence is a cold bias (~-0.5°C) over most of the Tasman Sea in eORCA025. The Tasman Front, the EAUC and its continuation along the east coast of the New Zealand's North Island and Chatham Rise, are characterised by a positive temperature bias in the order of about 0.5°C in both models. This warm bias is a consequence of an excessive heat transport of the Tasman Front in both models. In NZ20 this warm bias around the North Island of New Zealand is enhanced, and exceeds 0.6°C. However, there is no warm bias in the EAC Extension for NZ20. In addition, the Tasman Sea has turned from a cold bias in eORCA025 to a slight warm bias in NZ20, which can be attributed to stronger transport of heat from EAC Extension into the Tasman Sea in NZ20. The overall temperature bias does not show a clear separation between subtropical and subantarctic waters as is seen in salinity.

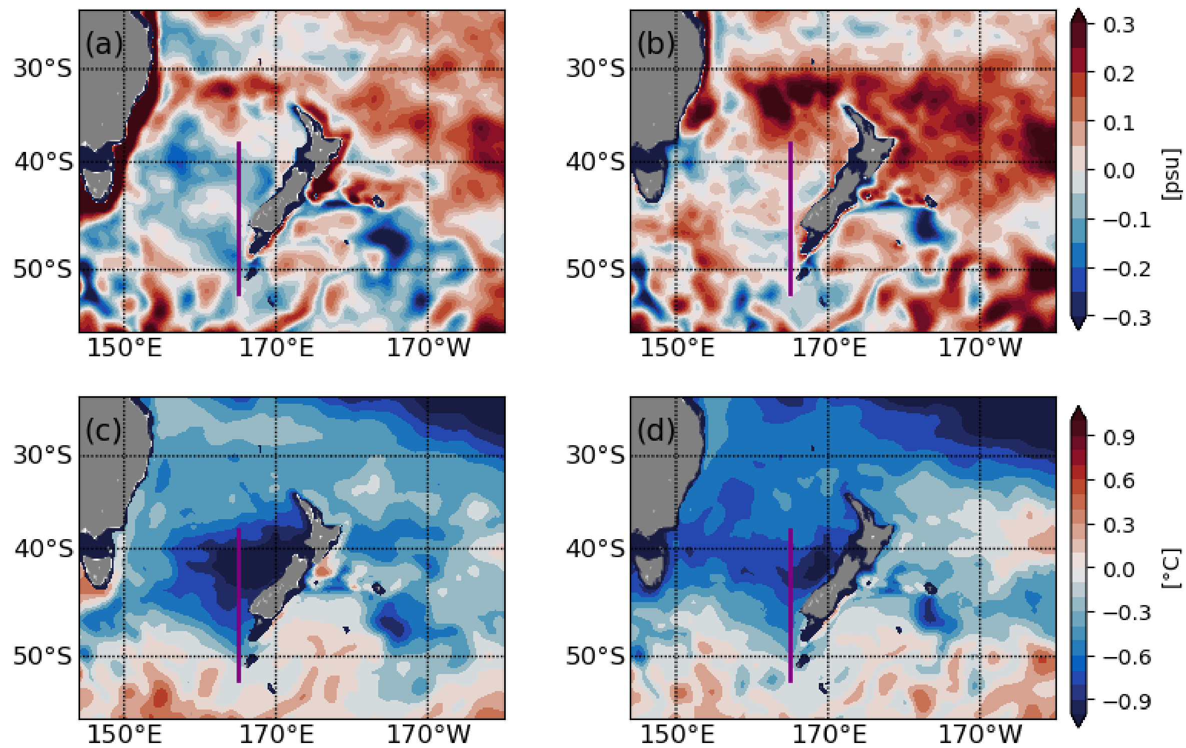

Figure 4. Upper 200m temperature (a-b) and salt (c-d) bias of eORCA025 (left panels) and NZ20 (right panels) against Argo over the period from 2004 to 2018. The purple line (165°E) marks the section used to investigate the impact of model biases on the STF detection (Figure 7).

As shown in Figure 3, both models experience a large-scale fresh bias in the Tasman Sea, which extends further north into the subtropics. In particular, the eastern Tasman Sea is too fresh (>-0.3 psu) in eORCA025 (Figure 4c), while the bias is more widely distributed over the Tasman Sea in NZ20. In contrast to the subtropical region, the subantarctic region, south of 50°S, is characterised by a weak positive salinity bias in both models.

As a consequence of the mesoscale eddies in NZ20, the transport of heat in eORCA025 and NZ20 differs, contributing to variations in the biases. The heat transport associated with the EAC is around 15% larger in NZ20 (Table 2). On the other hand, eORCA025 carries around 10% more heat in the EAC Extension to the south than NZ20, while NZ20 transports 4% more heat to the east in the Tasman Front. These numbers reflect differing heat pathways between NZ20 and eORCA025. The larger heat transport of the EAC and Tasman Front in NZ20 compared with eORCA025 contribute to the larger warm biases around the North Island of New Zealand in NZ20. Despite this enhanced bias in NZ20, the bias in the STF region is smaller; in particular, the cold bias over the Tasman Sea is reduced, which leads to a better representation of the STF location in NZ20 (see Section 4.1). This improvement is the result of larger heat transport into the Tasman Sea in NZ20, when comparing net heat transport across Tasman North and South sections (see section below).

3.4 Control sections

The following paragraph describes the model performance along 3 control sections within the high-resolution domain. The first two sections enclose the Tasman Sea (Tasman North and South sections) and are used to compare the transport of heat and freshwater into the Tasman Sea, which will be later linked to variability in the STF. The 3rd section, a meridional section at 165°E across the STF where the biases are largest, is used to illustrate the location of the STF and assess the model performance against Argo.

3.4.1 Tasman North section

Within the surface 500 m the modelled temperatures show a horizontal gradient, with warmer temperatures near the Australian coast and colder temperatures near New Zealand (Figure 5). The upper 100 m between 500 km and 2500 km are about 0.1°C warmer in NZ20 than in eORCA025 (Figure 5g), while the layer down to 250 m is about 0.1°C colder. Below 250 m the temperature difference between NZ20 and eORCA025 is at a maximum, with temperatures more than 0.5°C warmer in NZ20 near both continental slopes. This warm anomaly in NZ20 can be explained by the 15% heat transport increase in the EAC compared with eORCA025, carrying more warm water into the Tasman Sea. The heat transport across the Tasman North and South sections does not compensate for this enhanced inflow of heat into the Tasman Sea in NZ20 (Table 2). The salinity distribution of both models shows a similar horizontal temperature gradient, with high salinity near the Australian Coast (Figure 5h). The salinity minimum of Antarctic Intermediate Water can be seen in both models at around 1000 m depth. The upper 250 m in NZ20 appear to be fresher than in eORCA025, while the layer between 250 m to 1000 m is saltier (Figure 5h), similar to the temperature, and related to the different transports of freshwater within the EAC by the different models.

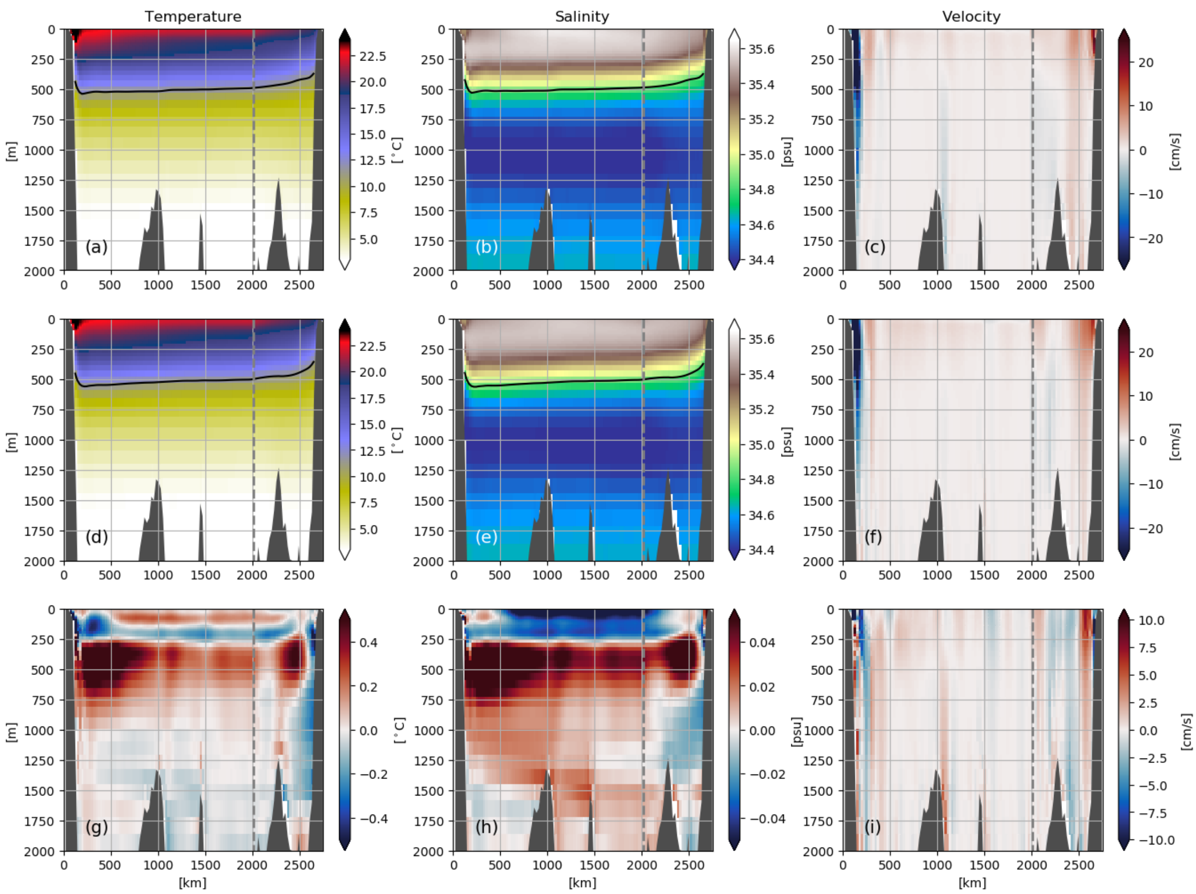

Figure 5. Time mean modelled temperature, salinity, cross section velocity along the Tasman North section for eORCA025 (top panels), NZ20 (middle panels) and NZ20 minus eORCA025 (bottom panels) for the period 1980 to 2018. The section starts at the Australian coast (0km) and ends at the northern tip of New Zealand (2700km). Black contour shows the 11°C/34.8 psu contour. The dashed line marks the where the zonal section turns to a meridional section.

The velocity structure is similar in both models (Figure 5c,f). The EAC occupies the upper 1500 m near the Australian coast, with velocities exceeding 20 cm/s in this long-term average. Observations have reported velocities up to 130 cm/s on subinertial time scales (Roughan and Middleton 2004). The remaining section is mainly characterised by outflow from the Tasman Sea, with a peak near New Zealand where the Tasman Front leaves the domain. The difference in cross section velocities shows a stronger EAC and larger outflow from the Tasman Sea until 2100 km in NZ20 (Figure 5j). The representation of the Tasman Front near New Zealand differs between the models. In eORCA025 it appears that the Tasman Front has one offshore branch at around 2400 km and a strong boundary current at the shelf of New Zealand and clear separation between both transport branches. In NZ20 the Tasman Front appears more concentrated towards New Zealand with increasing flows toward the coast, as suggested by the difference plot.

Mean transports of volume, heat and freshwater are in the range of observed estimates and other modelling studies (Table 2). The net volume transport is -6.3 Sv and -6.1 Sv in eORCA025 and NZ20, respectively; and the net heat transport is calculated to be -0.318 to -0.305 PW (1 PW = 10^{15} W). Thus, southward heat transport through the Tasman Sea in eORCA025 is stronger despite NZ20 showing a larger heat transport in the EAC. These differences suggest that the stronger EAC heat transport in NZ20 is overcompensated for by the enhanced recirculation east of the EAC and the Tasman Front back to the Pacific Ocean, which leads to a lower net heat transport in NZ20 compared to eORCA025 through the Tasman North section.

	Volume [Sv]	Heat transport [PW] (1 PW = 10^{15} W)	Freshwater transport [Sv]
Tasman North eORCA025	-6.3	-0.3184	-0.061
Tasman North NZ20	-6.1	-0.3059	-0.058
Tasman South eORCA025	-5.8	-0.1964	-0.023
Tasman South NZ20	-5.7	-0.1731	-0.029
EAC Observation	-25 to -37 Sv (Ridgway and Dunn 2003) -22 (Mata et al. 2000) -22 (Sloyan et al. 2016)		
EAC eORCA025	-19.3	-1.2593	0.145
EAC NZ20	-19.8	-1.4868	0.197
Tasman Front Observation	13 Sv (Ridgway and Dunn 2003) 8 (Stanton 2010)		
Tasman Front eORCA025	11.3	0.6218	-0.10
Tasman Front NZ20	9.7	0.644	-0.13
STG eORCA025	1.6	0.319	-0.09
STG NZ20	3.9	0.536	-0.11
EAC Extension Observation	-19 Sv (Ridgway and Dunn 2003)		
EAC Extension eORCA025	-9.4	-0.3245	-0.051
EAC Extension NZ20	-8.6	-0.2931	-0.047

Table 2: Time mean model transports (1980-2018) and observational estimates for Tasman North section, Tasman South section, East Australian Current (EAC), Tasman Front, subtropical gyre (STG) and East Australian Extension.

3.4.2 Tasman South section

The Tasman South section runs in the zonal direction along 43°S across the Tasman Sea. Like the Tasman North section, a horizontal gradient in temperatures is present within the upper 250 m (Figure 6 a,d). eORCA025 is > 0.5 °C warmer than NZ20 in the EAC Extension region, up to 200 km offshore

(Figure 6g). In contrast NZ20 is about 0.2-0.4 °C warmer in the upper 500 m from 200 km onwards across the entire Tasman Sea, but colder until 1250 m.

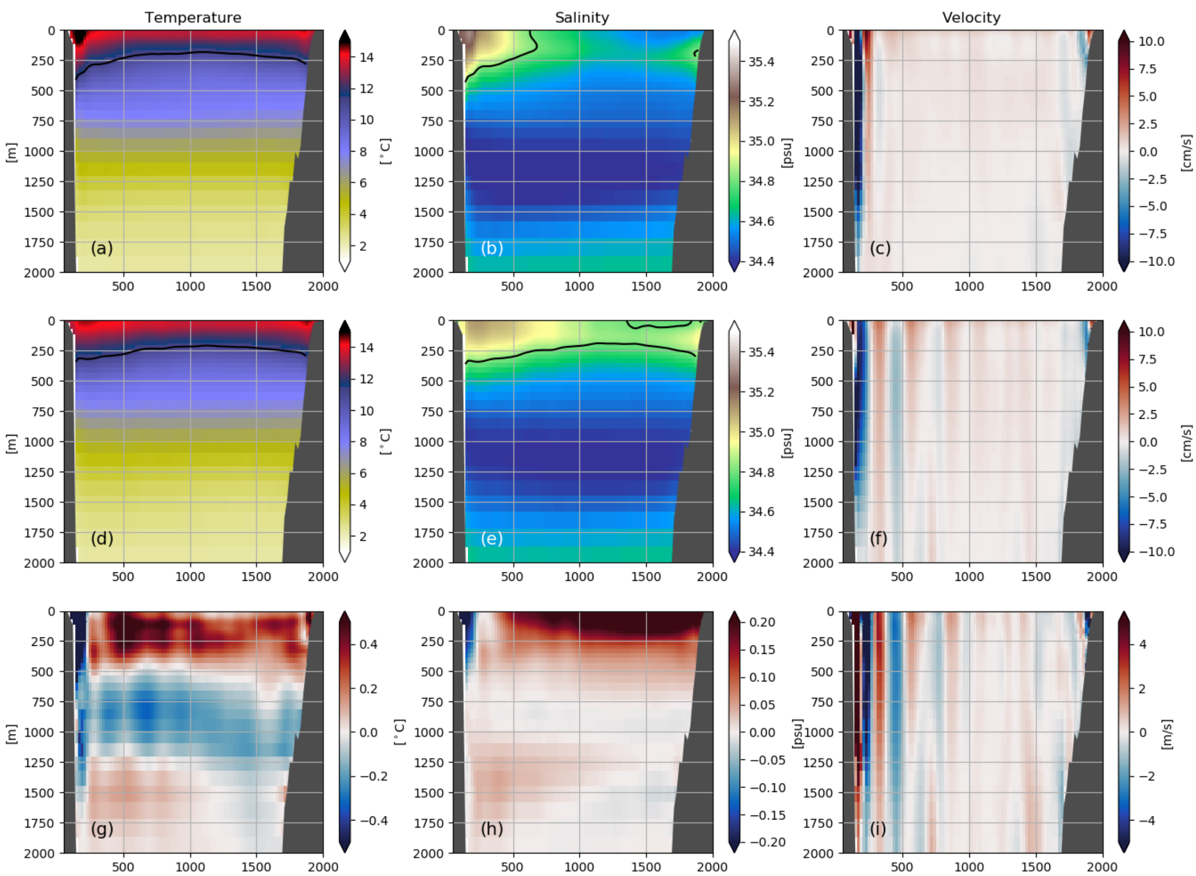

Figure 6. Time mean modelled temperature, salinity, cross section velocity along the Tasman South section for eORCA025 (top panels), NZ20 (middle panels) and NZ20 minus eORCA025 (bottom panels) for the period 1980 to 2018. Black contour shows the 11°C/34.8 psu contour.

The salinity distribution shows saltier regions on both continental shelves (Figure 6 b,e). The maxima near New Zealand is attributed to the flow associated with the STF as part of the localised Fiordland Current along the New Zealand's west coast of the South Island (Chandler, Bowen, and Smith 2019). eORCA025 has higher salinity in the EAC Extension, similar to the temperature signal, while salinity is higher elsewhere in NZ20 (Figure 6h). The negative difference in temperature and salinity within the EAC Extension can be linked to the overly stable EAC Extension in eORCA025. In NZ20 the EAC Extension is dominated by eddies, resulting in stronger transport of heat and salt into the interior of the Tasman Sea, producing a positive difference in temperature and salinity compared to eORCA025. This difference is also evident in the meridional velocities in both models, where the EAC Extension is concentrated close to the coast of Tasmania in eORCA025 compared with NZ20. Over most of the Tasman South section velocities in eORCA025 are uniformly northward, while NZ20 exhibits more zonal structures, and bands due to meandering currents. At the New Zealand coast, a weak southward transport can be seen, which is associated with the Fiordland Current flowing south feeding the Southland Current on the east coast of the New Zealand's South Island (Figure 6 c,f).

The imbalance of volume transports between Tasman North and South section varies between 1.5 – 3% relative to the transport across the Tasman North section due evaporation and transports through Brass and Cook Strait (Table 2). For heat transport it varies between 38 to 43% for eORCA025 and NZ20, respectively. Despite the lower net heat transports in NZ20 its imbalance is larger and leads to a reduction of the cold bias compared to eORCA025 over the Tasman Sea.

3.4.3 165° E section

This meridional section is used as an example to illustrate the location of the STF_{TEMP} and STF_{SALT} in the Tasman Sea from Argo and both models (Figure 7). This location also allows us to measure the impact of the model bias, since the salinity bias in this region is large (Figure 4). The time-mean 11°C isotherms of Argo, eORCA025 and NZ20 are shown in Figure 7a, with the ±1°C range shaded. Over the upper 200 m there is a good agreement between all data sets. The location of the STF_{TEMP} based on the 11°C isotherm (hexagons) in NZ20 and Argo are nearly a perfect match, while the STF_{TEMP} in eORCA025 is shifted slightly north, since eORCA025 is slightly colder.

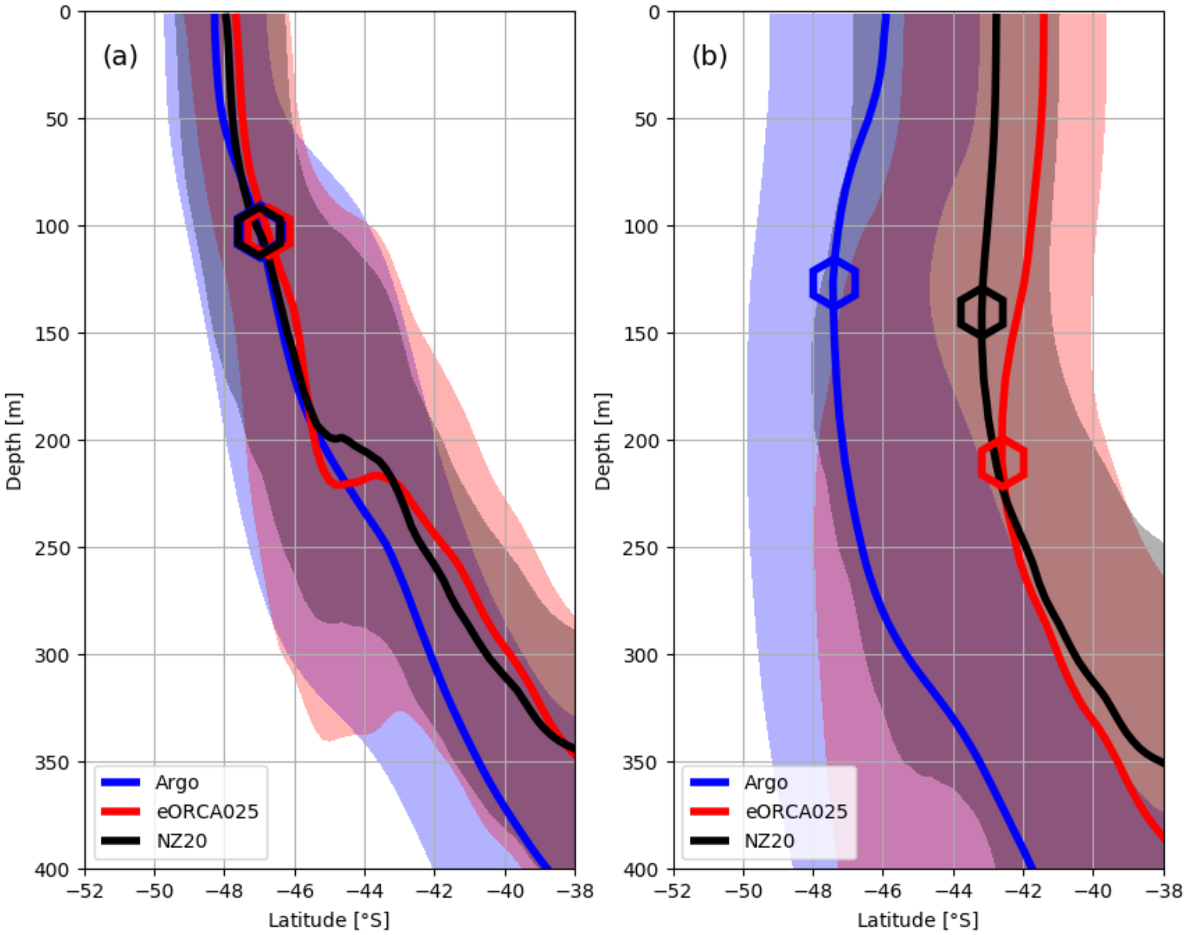

Figure 7. Meridional section along 165°E through the Tasman Sea. (a) Time mean (2004-2018) 11°C isotherm shown by the solid lines and ±1°C deviation by the color shading. (b) Time mean (2004-2018) 34.8 psu isohaline shown by the solid lines and ±0.2 psu deviation by the color shading. The hexagons show the location of the STF according to the isotherms and isohalines.

The salinity discrepancy between Argo and the models is larger. As seen in the salinity biases (Figure 4a-b), both models show a fresh bias in the subtropical waters over the surface 200 m of the Tasman Sea. The same behaviour is seen along this meridional section and the 34.8 psu isohaline is shifted around 4°-5° to the north in both models. Conversely, the vertical structure, and particularly the presence of a subsurface maxima, is consistent between Argo and both models. Argo and NZ20 show this subsurface maximum between 100 m and 150 m depth, while it is found around 220 m depth in eORCA025. This difference causes the STF_{SALT} to be slightly further south in eORCA025 compared with NZ20.

The model evaluation has demonstrated that NZ20 performs better in several STF-related diagnostics than eORCA025 (e.g. reduced model biases in the STF region). The main shortfall of eORCA025 is the overly stable EAC Extension, which contributes to temperature and salinity biases over the Tasman Sea and impacts the location of the STF in the model. In the remainder of this paper, we will therefore only present NZ20 results, which arguably performs better in simulating the STF.

4 Characterisation of the STF in space and time

In the following section we present the mean modelled STF location over our target region and compare it against observations. In addition, we also investigate the meridional variability from seasonal to interannual timescales of the STF and propose potential drivers of STF variability on interannual time scales.

4.1. Mean location of the STF

The mean location for the STF_{TEMP} and STF_{SALT} from Argo and NZ20 is shown over our target region in Figure 8. Since we use fixed temperature and salinity values over the entire domain, the STF detection around New Zealand comes with some caveats. Horizontal and vertical mixing within the boundary currents and freshwater input from rivers change the temperature and salinity structure along the coast. This issue becomes more relevant with increasing model resolution, when the boundary currents are better resolved. Consequently, the detection algorithm indicates that the STF passes through Cook Strait, which is an unrealistic consequence of our STF detection technique. Therefore, we discard the STF locations within 60 km of the New Zealand coast. Despite this limitation, there is agreement in the mean location of the STF_{TEMP} and STF_{SALT} between Argo and NZ20 and encourages us to accept this shortcoming for the sake of comparability of the results.

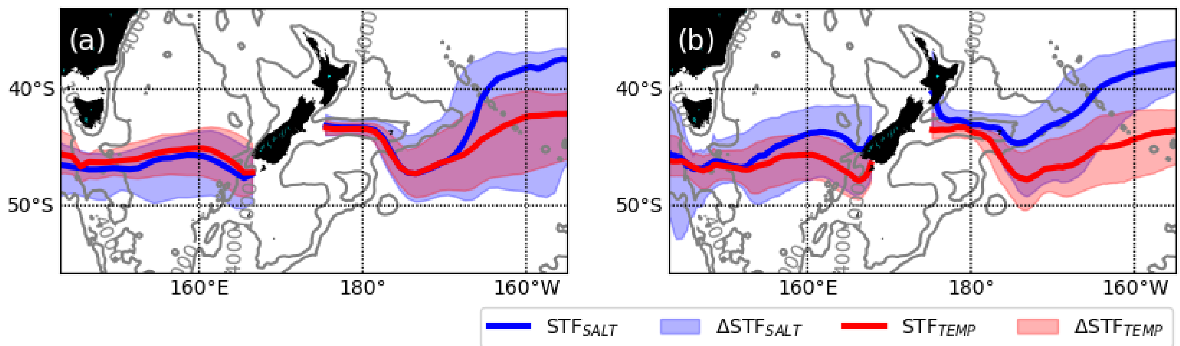

Figure 8. Time mean STF locations for Argo (a) and NZ20 (b) shown as solid lines for the period from 2004 to 2018. Colour shading in (a-c) shows the range in STF location with small deviation from temperature (±1 °C) and salinity (±0.2 psu) STF thresholds.

The STF_{TEMP} (red line and shading in Figure 8a-b) runs south of Tasmania across the Tasman Sea and south of New Zealand with little change in its latitudinal position. To the east of New Zealand, the STF_{TEMP} follows the Chatham Rise, then veers southeast by ~ 3-4° degrees in latitude, before veering northwards again. There is a good agreement between Argo and NZ20 for the location of the 11°C isotherm and the ±1°C range. Therefore, the location of the STF_{TEMP} is not sensitive to changes in the temperature values, indicated by a relative narrow band of the ±1° temperature envelope in most regions of the SW Pacific.

In Argo the STF_{SALT} is located about the same latitude as STF_{TEMP} over the Tasman Sea until 170°W, east of New Zealand (Figure 8a). Further to the east the salinity and temperature estimates of the STF diverge from each other and STF_{SALT} shifts northward, reaching latitudes of about 38°S at 160°W. The salinity envelope highlights several regions where the STF_{SALT} position is sensitive to the choice of the reference salinity. Over the Tasman Sea the envelope is around 5° wide. To the east of the New Zealand the corridor is initially very narrow (2°), but exceeds 15° east of the Chatham Rise at around 160°W. This large range at 160°W is caused by a split in the flow of subtropical waters downstream from the Chatham Rise, and the subsurface maxima in salinity. A southern branch continues slightly north of 50°S, while a northern branch follows the 4000m depth contour north, until this contour turns northwest around 170°W (not shown). The envelope is larger to the south of the mean STF_{SALT} location (34.8 psu), which reflects a weaker salinity gradient within the subantarctic water than in the subtropical water. NZ20 is able to simulate the position of STF_{SALT} which is seen in Argo but displays a northward shift of the STF_{SALT} of up to 4° latitude in some regions (e.g. near Fiordland and east of the Chatham Rise, Figure 8b). These differences increase to the east, away from bathymetric constraints. In eORCA025 these differences are larger, due to the larger model salinity biases in these regions (not shown).

4.2. Seasonal variability of the STF

In the following section we investigate the seasonal meridional variability using Hovmöller plots (Figure 9). The seasonal variability for STF_{TEMP} is very coherent between Argo and NZ20 (Figure 9a-b). Argo and NZ20 both show a more northward location of STF_{TEMP} during austral winter months (July-October) reaching its most northern limit in September, indicated by the positive anomalies during this period. The southern-most STF_{TEMP} extent occurs during late austral summer, between February and May. The timing does not vary zonally, since this seasonal variability is dominated by surface radiative heating. On the other hand, the meridional range does vary zonally with a seasonal range of up to 4° latitude over the Tasman Sea, around 2° over Chatham Rise, and 6° further to the east in the South Pacific.

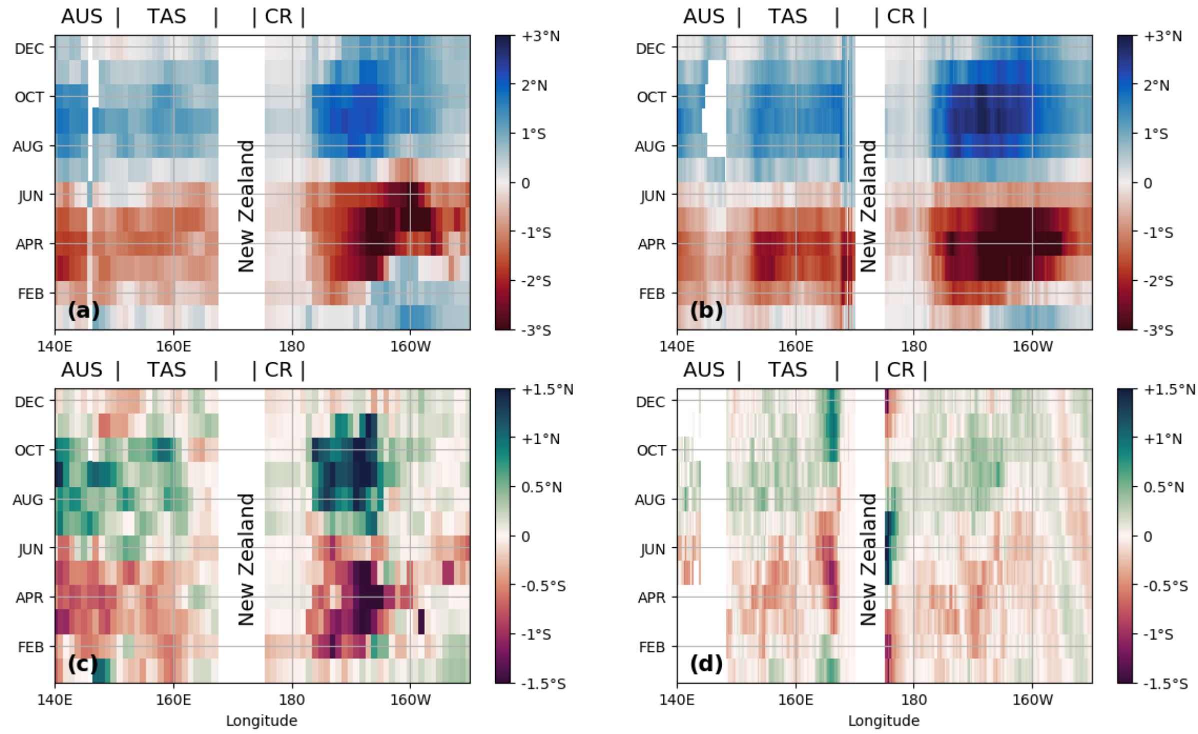

Figure 9. Seasonal meridional variation of the STF for Argo (left panels) and NZ20 (right panels) over the period 2004 to 2018. STF_{TEMP} (a, b) and STF_{SALT} (c, d). The zonal range of Australia (AUS), Tasman Sea (TAS) and Chatham Rise (CR) are shown by the respective labels on the top.

The Argo climatology for STF_{SALT} shows an overall seasonal range of about 2° over the Tasman Sea (Figure 9c-d), with a southward maximum during late austral summer (March-April). Over the Chatham Rise the range is reduced to 0.5°. East of Chatham Rise, in the South Pacific, the seasonal range increases to 3-4° in latitude until 160°W. NZ20 displays a smaller meridional seasonal range than Argo climatology, barely exceeding 1°. The model bias, the sea surface salinity restoring, and differences in the horizontal and vertical resolution between Argo and the model are likely contributing to this difference. Despite the weaker seasonal cycle in NZ20, both observations and models show a delay of the summer-time southward migration of 2-3 months near the west coast of New Zealand due to larger freshwater input during this time of the year from rivers and glacier melt. In this region, the southward maximum extent of STF_{SALT} occurs during June. This is when river flows are at their minimum, due to snow accumulation on the Southern Alps (Kerr 2013). East of the Chatham Rise we also observe a delayed southward STF_{SALT} maximum during late austral autumn in Argo and in NZ20 (although weaker). The delay increases when moving east. Results from STF_{TEMP} and STF_{SALT} suggest that the seasonal range is largest in the open ocean and is reduced near regions where the STF encounters shallow bathymetry.

4.3. Interannual variability of the STF

On interannual time scales, based on de-seasonalised annual means, we observe meridional shifts of the STF_{TEMP} and STF_{SALT} of about 2-4° from its mean location in Argo (Figure 10 a,c). The comparison of the model results to the Argo climatology is hampered by the short length of the Argo observational record which only starts in 2004. Over the Tasman Sea the Argo climatology shows a southward shift of the STF_{TEMP} of about 1-2° since 2004, but this is not zonally uniform. A similar tendency is present in STF$_{SALT}$ in this region, which suggests saltier and warmer subtropical waters flowing into this region, perhaps as a result of an southward expanding Super-Gyre (Yang et al. 2020). East of New Zealand the interannual variability is enhanced, and STF$_{TEMP}$ and STF$_{SALT}$ also show an overall southward tendency.

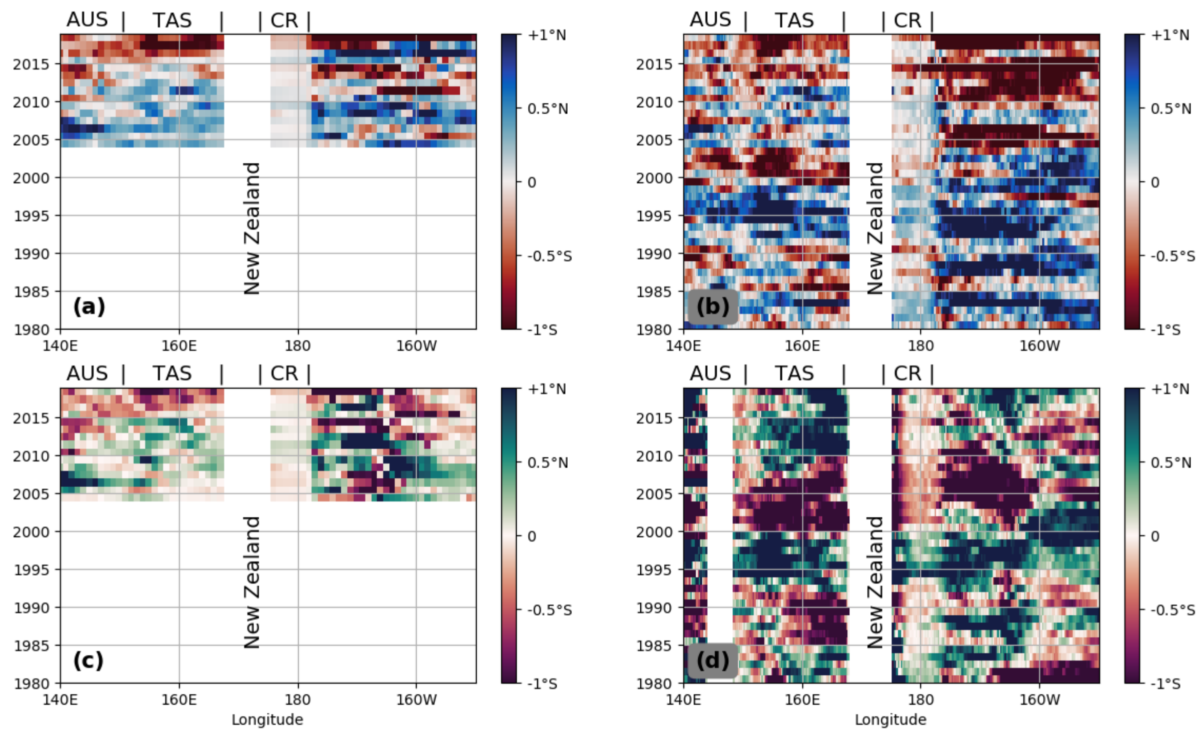

Figure 10 Interannual meridional variation of the STF for Argo (left panels) and NZ20 (right panels). over the period 1980 (2004, Argo) to 2018. STF$_{TEMP}$ (a, b) and STF$_{SALT}$ (c, d). The zonal range of Australia (AUS), Tasman Sea (TAS) and Chatham Rise (CR) are shown by the respective labels on the top.

NZ20 shows a similar southward tendency for the STF$_{TEMP}$ over this period (from 2004 to present) in the Tasman Sea, but no southward trend for STF$_{SALT}$ (Figure 10 b,d). Moreover, the longer STF timeseries from NZ20 suggests considerable variability on timescales of 5-10 years (Figure 10 b,d). For example, NZ20 simulates a northward shift of STF$_{TEMP}$ and STF$_{SALT}$ from 1994 to 2000 of about 1° over the entire Tasman Sea with a reversed southward shift from 2000 to 2004 of about -0.75 to -1° in STF$_{TEMP}$ and STF$_{SALT}$. Observations along the SR3 hydrographic section, south of Tasmania, also found a northward shift of the STF during 1996 (Sokolov and Rintoul 2002). These large signals are also visible east of New Zealand, but with a delay of up to two years. The coherence of these shifts of the STF, temporally and spatially east and west of New Zealand, suggest basin-wide changes in the subtropical gyre circulation and the meridional transport and extent of subtropical water, which is investigated in the next section. The large interannual variability in the model hindcast suggest that caution is required to identify trends in the relatively short observational records.

4.4. Upper 500 m Heat and FW content changes

In the following section we investigate the drivers of the meridional shifts of the STF, linking them to dynamical changes in the transport of heat and freshwater into the Tasman Sea (the enclosed region of Tasman North and South sections) and changes in the South Pacific subtropical gyre circulation. We focus on the NZ20 model results, as we cannot directly estimate transports from the observations. Figure 11a shows the freshwater transport anomalies across both control sections, Tasman North and

South. The timeseries show large interannual variability, exceeding ±0.05 Sv. With a few exceptions, Tasman North section shows the largest freshwater transport anomalies. The period from 1986 to 1995 is significant, because freshwater transport anomalies of the Tasman North section are large and persistently southward (with the exception of 1992 and 1993). The opposite is true for the period 1996-1999. A second period with strong southward freshwater anomalies in the Tasman North transports is the period 2005 to 2011. In comparison, the Tasman South freshwater transport anomalies are lower and therefore do not compensate for the Tasman North transport anomalies.

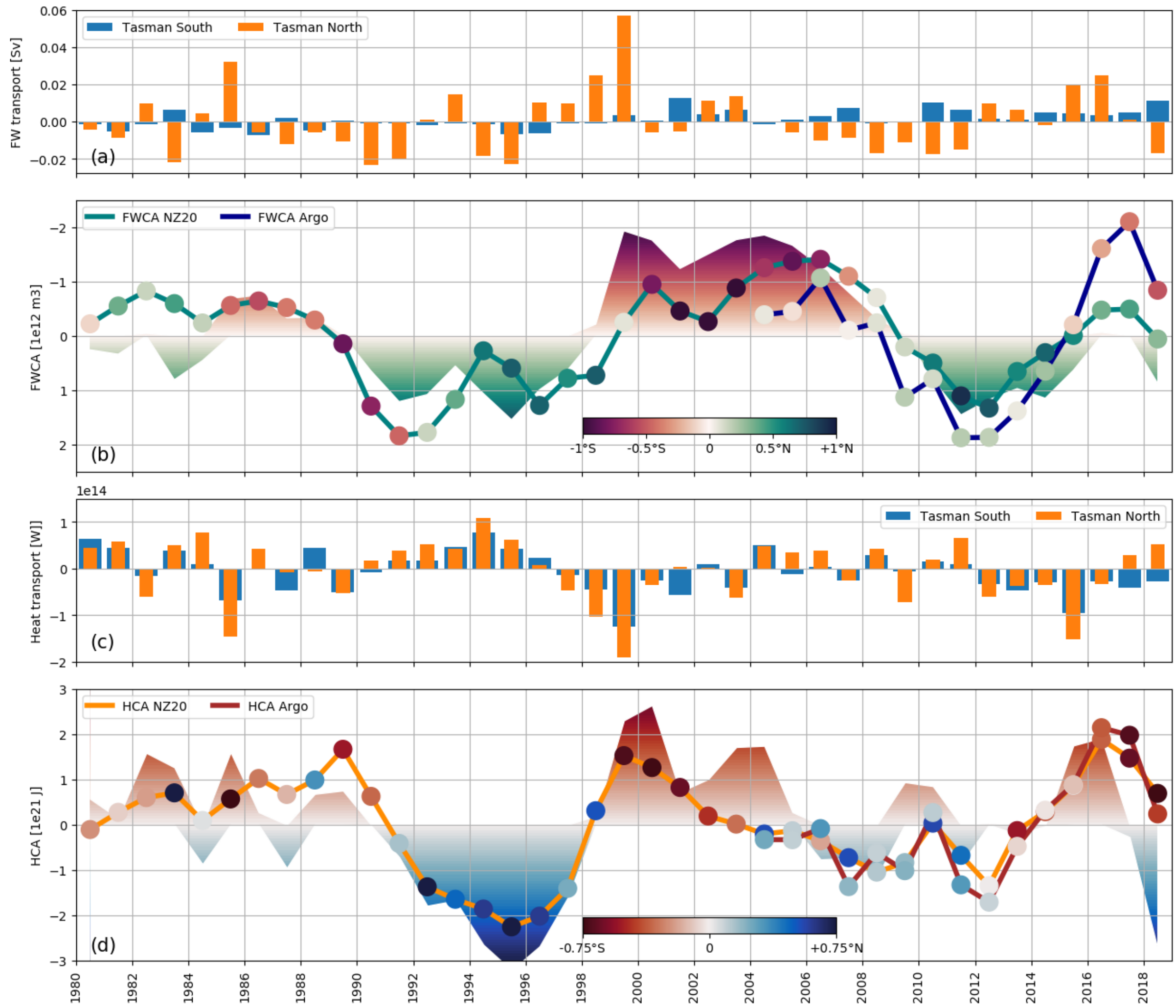

Figure 11. Time series of annual integrated 0 – 500m mean (a) freshwater transport across TN and TS, (b) estimated freshwater content based on freshwater transports (color shading), true freshwater content anomaly (FWCA, S_{ref}=34.8) from NZ20 (teal) and Argo (dark blue). The color-coded dots show the meridional anomaly of the STF locations over the Tasman Sea. (c) and (d) the same diagnostic but for heat transport and heat content anomaly (HCA).

We estimate the freshwater content anomaly in NZ20 based on the 0 – 500m freshwater transport anomalies over the Tasman Sea (enclosed region of Tasman North and South), assuming a constant surface flux. We compare this estimate (color shading) against the true modelled (solid teal line) 0 – 500m freshwater content anomalies in Figure 11b. The estimated freshwater content anomaly can reproduce most interannual to decadal signals of the modelled freshwater content anomalies, which indicates that interannual variability of surface fluxes are of minor importance for the overall budget. Between 1986-1995 the freshwater content anomaly becomes progressively more positive and reaches a maximum in 1995 of about $1.2\times10^{12}m^3$, before turning negative with a minimum of around $-2\times10^{12}m^3$ in 1999 (note the reversed y-axis). Over the period from 2005 to 2011 the freshwater content increases constantly until 2011, reaching similar values as in 1995. Over the last few years (2015-2017) freshwater content was nearly neutral with a positive anomaly in 2018. The Argo freshwater content anomaly (blue line) shows the same decadal signals, but with a lower freshwater content over the past few years (2015-2018). Freshwater content anomaly is correlated with the STF_{SALT} over the Tasman sector, as indicated by color-coded dots in the freshwater content timeseries.

Similar to the freshwater transports, the Tasman North heat transports are larger than the Tasman South, which highlights their importance as a driver for variability, and indicates that the Tasman Sea loses heat to the atmosphere (Figure 11c). We find co-variability between freshwater and heat content transport. The period from 1990 to 1996 can be identified as period with persistent northward heat transport anomalies, with the opposite phase from 1997 to 2000, and 2012 to 2016. The remaining timeseries shows larger year to year variability, compared with the freshwater transports.

The NZ20 estimated heat content anomalies (color shading Figure 11d), based on the heat transport in the upper 500 m layer, captures the true modelled heat content anomalies (orange curve). The Argo timeseries (red curve) is very similar to the modelled heat content changes. We can identify a persistent cold period from 1990-1998, with mainly northward heat transport anomalies and Tasman North exceeding Tasman South, causing the heat content in the Tasman Sea to drop. Some of this cold period can be linked to the eruption of Pinatubo in 1991, which led to a widespread cool. The heat content anomaly minimum is reached in 1995 with -3×10^{21} J, but rebounds rapidly to a positive heat content anomaly with a maximum of around 2×10^{21} J in 2000. Since 2000 the heat content displays a negative trend until 2012, when it reversed and displays elevated positive anomalies for the period 2015 and 2016. Some of this negative heat content trend from 2000-2012 might be linked to a negative Interdecadal Oscillation and positive phase since 2011. For 2017 and 2018 the estimated heat content has declined to similar values as seen in 1995, with the true modelled heat content (solid lines) also following this trend.

The NZ20 model simulations demonstrate that heat and freshwater transports through the northern boundary of the Tasman Sea co-vary. Furthermore, heat and freshwater content over the region show similar long-term variability, as does the position of both STF_{TEMP} and STF_{SALT}. This result is consistent with the hypothesis that warm and saline anomalies are advected into the Tasman Sea, and thereby act to shift the STF southwards, and conversely cool and fresh anomalies result in a northward shift in the STF in this region.

4.5. Local wind-stress curl as driver for variability

Estimated annual heat content anomalies in the upper 500 m display a positive relationship with SST over most of the SW Pacific; this relationship is most significant over the Tasman Sea (Figure 12a). Local correlation exceeds 0.6 and extends to the south of the Tasman Sea and Australia towards the Indian Ocean. Positive correlations are also obtained between the heat content and SSH (Figure 12b). Large, significant correlations are obtained over the central and eastern Tasman Sea and extend into the Southern Ocean. This positive correlation over the Tasman Sea is a result of enhanced wind stress curl and subsequent Ekman convergence (Figure 12c), particularly in the eastern Tasman Sea. However, correlations in other regions are not significant.

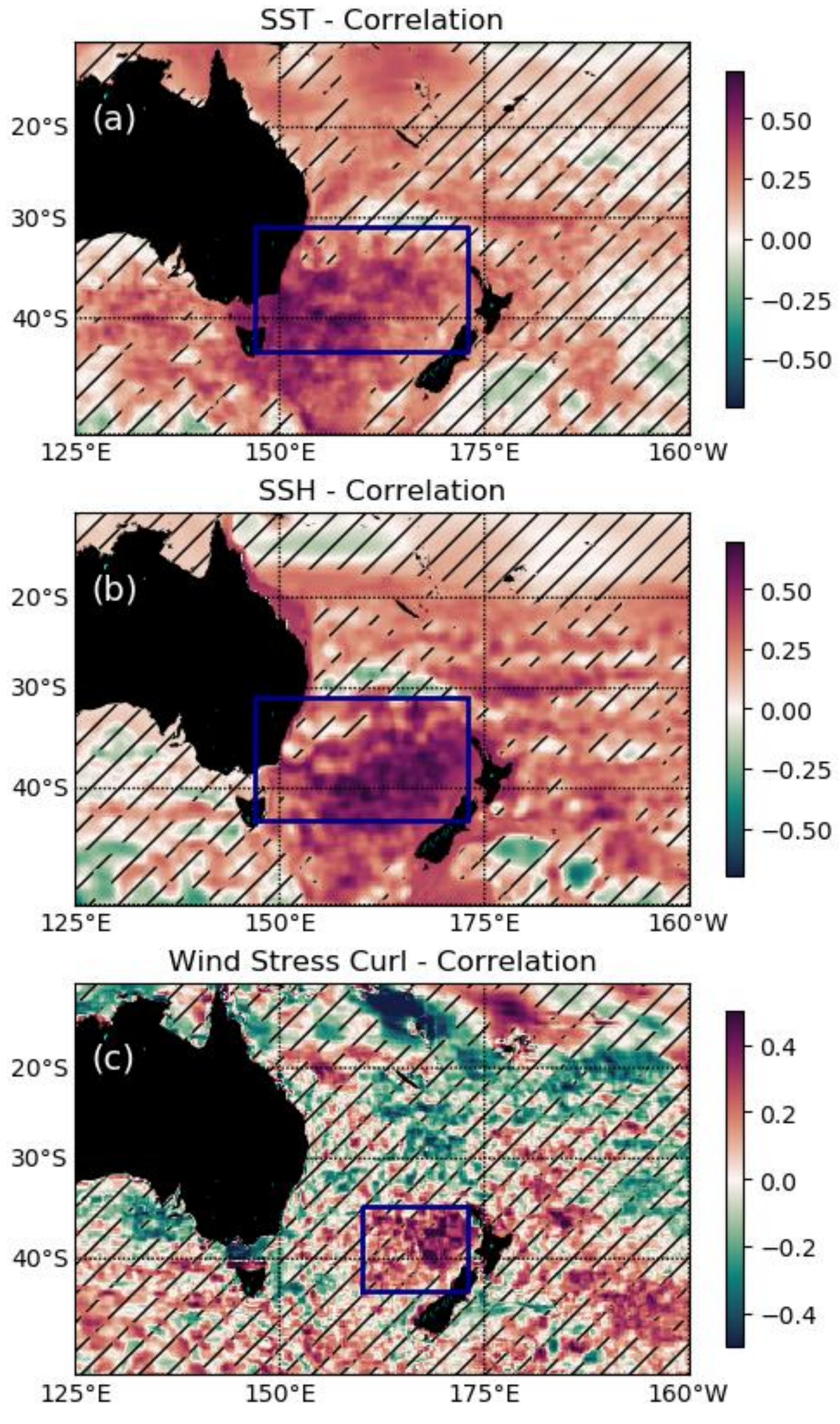

Figure 12. Correlation between integrated 0 – 500m Tasman Sea heat content proxy and SST (a), SSH (b) and wind stress curl (c) over the period from 1980 to 2018. Blue boxes mark regions for area averages for Figure 13. Hashed regions show not significant correlations.

The area-averaged timeseries of SST, SSH and wind stress curl over the highlighted regions in Figure 12 are shown in Figure 13. SST and SSH anomalies follow the estimated heat content anomalies in the upper 500m. Wind stress curl (purple bars) exhibits larger variability than SST and SSH, but strong and/or persistent heat content anomalies can be linked to them. Cold periods are characterised by negative wind stress curl anomalies, when Ekman divergence causes heat content to decrease, while warm periods are characterised by positive wind stress curl anomalies, when Ekman convergence increase the heat content.

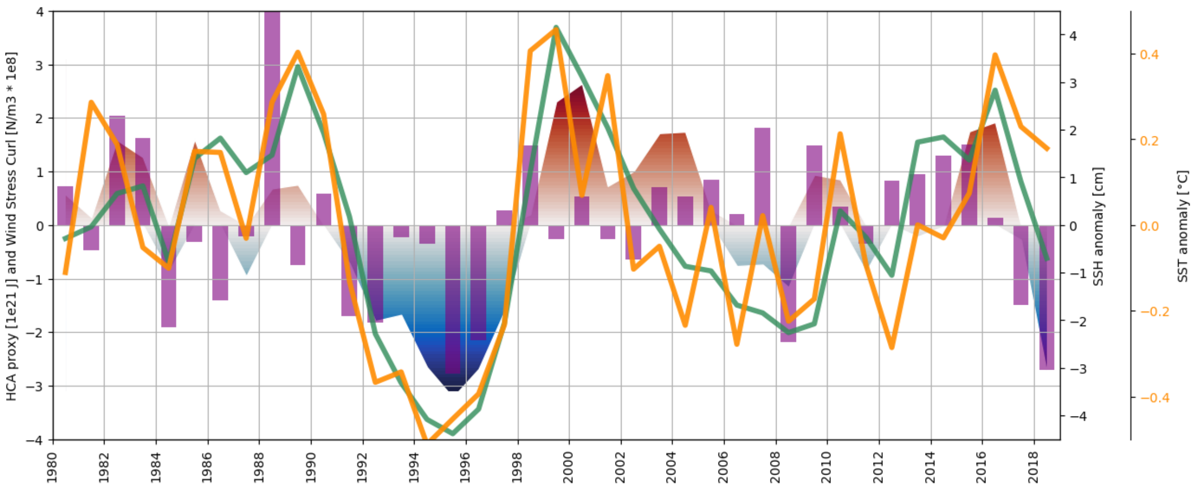

Figure 13. Estimated 0 – 500m Tasman Sea heat content anomaly (HCA) represented by the color shading. Area averaged SSH (green line, first right y-axis), SST (orange, second right y-axis) and winds stress curl (purple bars, left y axis). Regions over which the quantities have been averaged are shown in Figure 12.

5 Discussion and conclusion

We have demonstrated that the high-resolution (1/20°) two-way nested model (NZ20) captures the oceanic circulation around New Zealand better than a global ¼° model (eORCA025) which leads to reduced model biases of temperature and salinity (Figure 4). We further showed that NZ20 is capable of simulating STF variability on seasonal to interannual timescales in agreement with Argo and other observations (Figure 10). For example, the reported northward shift of the STF_{TEMP} along the SR3 hydrographic section south of Tasmania in 1996 (Sokolov and Rintoul 2002) is well represented in NZ20. This result suggests that simulating the boundary current dynamics and mesoscale eddies is important to capture the temporal variation. Other modelling studies from this region have come to similar conclusions, with improved performance of models with higher model resolution (Bull et al. 2017; Oliver, O'Kane, and Holbrook 2015; Kiss et al. 2020).

The data from Argo and the NZ20 model show that the STF around New Zealand varies not only on seasonal time scales, but also on interannual to decadal time scales. However, the seasonal cycle dominates the meridional shift of the STF, which can reach up to 6° (650 km) in the open ocean as a result of seasonal atmospheric heating. In terms of STF seasonal variability, our results are consistent with previous studies, which suggest seasonal shifts between 1-4° in the Southern Ocean (Graham et al. 2012; Sallée, Speer, and Morrow 2008; Sokolov and Rintoul 2009b; Kim and Orsi 2014). These shifts in the STF are significantly reduced in regions where the STF encounters bathymetry, such as the Chatham Rise (Figure 9 and 10). Along the Chatham Rise we observe large transports of adjacent subtropical and subantarctic water masses, which cause large persistent gradients in water mass properties. The cause appears to be the focusing effect of bathymetry on currents along the Chatham Rise to lock the STF to this feature (Sutton 2001). To the east of Chatham Rise the bathymetry drops and the flow forms eddies and meanders, which increase the variability of the STF and potentially make the STF more susceptible to external climate forcing and trends (Figure 8). This finding is consistent with previous studies showing larger variability of fronts in the open ocean compared with fronts closer to steep topography (Sallée, Speer, and Morrow 2008; Sokolov and Rintoul 2009b, 2007; Graham et al. 2012; Fernandez, Bowen, and Carter 2014).

The Argo data show a southward trend of the STF position since 2004 in the Tasman Sea and east of the Chatham Rise. However, the long hindcast of NZ20 exhibits large meridional shifts of the STF in these open ocean regions on interannual to decadal time scales and raises the question of how much of the observed southward STF trend in Argo from 2004 onward, is part of interannual to decadal variability. The model results indicate that these trends in the position of the STF south of the Tasman Sea are influenced by heat and freshwater content anomalies in the Tasman Sea. Modulations in the Tasman Sea heat and freshwater content impact the location of the 11° isotherm and the 34.8 psu isohaline, which have been used to define the STF, following earlier studies (Orsi, Whitworth, and Nowlin 1995). Although heat and freshwater content are linked with isotherms and isohalines, the relationship is indirect, since the STF is located south of the Tasman Sea and changes in isotherms and isohalines do not necessarily imply heat and freshwater content changes.

The modelling results suggest that the heat and freshwater anomalies are dominated by oceanic transport and are a consequence of wind stress curl anomalies in the eastern Tasman Sea, which drive Ekman convergence or divergence. During phases of positive wind stress curl, the Ekman transport converges, causing heat content to increase and the STF to move southward. The opposite behaviour has been found for periods with negative wind stress curl with increased freshwater content, due to Ekman divergences, shifting the STF northward. The anomalous transports within the EAC and across the northern boundary of the Tasman Sea are therefore the major driver of the STF shifts, while the magnitude of transport variability across the southern boundary is much smaller. Since the STF variability is forced by local drivers, it is imperative that ocean models can capture the local and regional scales realistically. There is no apparent relationship between the STF variability and large-scale climate drivers such as El Nino Southern Oscillation, Interdecadal Pacific Oscillation and Pacific Decadal Oscillation. The limited influence of large-scale climate drivers on Tasman Sea variability (e.g. variability of the EAC and heat content) agrees with earlier studies (Ridgway and Dunn 2007; Behrens, Fernandez, and Sutton 2019). Further work is required to determine the origin of the local wind stress curl anomalies, which drive anomalous oceanic transports.

In conclusion we have shown that a high-resolution ocean model is able to capture observed STF variability in the Tasman Sea and around New Zealand. The STF variability is largest on seasonal time scales and in regions away from shallow bathymetry. The interannual to decadal STF variability south of the Tasman Sea is linked to fluctuations of heat and freshwater content within the Tasman Sea as a consequence of local wind stress curl anomalies and Ekman transport.

Connecting the meridional shifts of the STF to basin scale changes in heat and freshwater allows for a more robust understanding of the drivers of variability, such as wind stress curl, on longer time scales. Furthermore, this improved understanding may provide a new paleo proxy for STF changes, using paleo SST from the northern Tasman Sea (e.g. from corals or marine sediment cores) to estimate potential changes in the paleo-STF. A better knowledge of how the STF responds to external drivers is also vital for gauging future changes in the position of the STF.

6 Acknowledgements

This paper obtained funding and support through Royal Society Marsden Fund (NIW1701) and the Ministry of Business Innovation and Employment Deep South National Science Challenge projects. We would like to acknowledge the NeSI High Performance Computing Facility team for their technical support. Finally, I would like to acknowledge my partner and son. NZ20 has been specifically developed to study the dynamics of the STF and oceanic variability around New Zealand, as part of the Stormy Seas project (https://niwa.co.nz/climate/research-projects/the-stormy-seas-project ,as part of NIW1701) and complements the development of New Zealand's Earth System Model (NZESM, (Behrens et al. 2019; Williams et al. 2016)), which is also based on a nested setup. AMcCH and MHE are supported by the Australian Research Council (ARC), including the ARC Centre of Excellence for Climate Extremes. The data used for this manuscript can be publicly accessed through following link https://doi.org/10.5281/zenodo.3755270 .

7 References

Barnier, B., G. Madec, T. Penduff, J. M. Molines, A. M. Treguier, J. Le Sommer, A. Beckmann, A. Biastoch, C. Boning, J. Dengg, C. Derval, E. Durand, S. Gulev, E. Remy, C. Talandier, S. Theetten, M. Maltrud, J. McClean, and B. De Cuevas. 2006. 'Impact of partial steps and momentum advection schemes in a global ocean circulation model at eddy-permitting resolution', *Ocean Dynamics*, 56: 543-67.

Behrens, Erik, Denise Fernandez, and Philip Sutton. 2019. 'Meridional oceanic heat transport influences marine heatwaves in the Tasman Sea on interannual to decadal timescales', *Frontiers in Marine Science*, 6: 228.

Behrens, Erik, Jonny Williams, Olaf Morgenstern, Phil J. Sutton, Graham Rickard, and Mike Williams. 2019. 'Local Grid Refinement in New Zealand's Earth System Model: Tasman Sea Ocean Circulation Improvements and Super-Gyre Circulation Implications', *Earth and Space Science Open Archive*.

Belkin, I. M., and P. Cornillon. 2003. 'SST fronts of the Pacific coastal and marginal seas', *Pacific Oceanography*, 1: 90-113.

Belkin, I. M., and A. L. Gordon. 1996. 'Southern Ocean fronts from the Greenwich meridian to Tasmania', *Journal of Geophysical Research-Oceans*, 101: 3675-96.

Bull, C. Y. S., A. E. Kiss, N. C. Jourdain, M. H. England, and E. van Sebille. 2017. 'Wind Forced Variability in Eddy Formation, Eddy Shedding, and the Separation of the East Australian Current', *Journal of Geophysical Research-Oceans*, 122: 9980-98.

Burls, N. J., and C. J. C. Reason. 2006. 'Sea surface temperature fronts in the midlatitude South Atlantic revealed by using microwave satellite data', *Journal of Geophysical Research-Oceans*, 111.

Butler, E. C. V., J. A. Butt, E. J. Lindstrom, P. C. Tildesley, S. Pickmere, and W. F. Vincent. 1992. 'Oceanography of the Subtropical Convergence Zone around Southern New-Zealand', *New Zealand Journal of Marine and Freshwater Research*, 26: 131-54.

Cai, W. 2006. 'Antarctic ozone depletion causes an intensification of the Southern Ocean super-gyre circulation', *Geophysical Research Letters*, 33: L03712.

Chandler, Mitchell, Melissa Bowen, and Robert Owain Smith. 2019. 'The Fiordland Current, southwest New Zealand: mean, variability, and trends', *New Zealand Journal of Marine and Freshwater Research*: 1-21.

Chiswell, S. M. 2001. 'Eddy energetics in the Subtropical Front over the Chatham Rise, New Zealand', *New Zealand Journal of Marine and Freshwater Research*, 35: 1-15.

———. 2002. 'Temperature and salinity mean and variability within the Subtropical Front over the Chatham Rise, New Zealand', *New Zealand Journal of Marine and Freshwater Research*, 36: 281-98.

De Boer, Agatha M., Robert M. Graham, Matthew D. Thomas, and Karen E. Kohfeld. 2013. 'The control of the Southern Hemisphere Westerlies on the position of the Subtropical Front', *Journal of Geophysical Research: Oceans*, 118: 5669-75.

Deacon, G. E. R. 1982. 'Physical and Biological Zonation in the Southern-Ocean', *Deep-Sea Research Part a-Oceanographic Research Papers*, 29: 1-15.

Debreu, L., C. Vouland, and E. Blayo. 2008. 'AGRIF: Adaptive grid refinement in Fortran', *Computers & Geosciences*, 34: 8-13.

Edwards, R. J., and W. J. Emery. 1982. 'Australasian Southern Ocean frontal stucture during summer 1976-77', *Marine and Freshwater Research*, 33: 3-22.

Fernandez, D., M. Bowen, and L. Carter. 2014. 'Intensification and variability of the confluence of subtropical and subantarctic boundary currents east of New Zealand', *Journal of Geophysical Research: Oceans*, 119: 1146--60.

Good, Simon A., Matthew J. Martin, and Nick A. Rayner. 2013. 'EN4: Quality controlled ocean temperature and salinity profiles and monthly objective analyses with uncertainty estimates', *Journal of Geophysical Research: Oceans*, 118: 6704--16.

Graham, R. M., and A. M. De Boer. 2013. 'The Dynamical Subtropical Front', *Journal of Geophysical Research-Oceans*, 118: 5676-85.

Graham, R. M., A. M. de Boer, K. J. Heywood, M. R. Chapman, and D. P. Stevens. 2012. 'Southern Ocean fronts: Controlled by wind or topography?', *Journal of Geophysical Research-Oceans*, 117: C08018.

Hamilton, L. J. 2006. 'Structure of the Subtropical Front in the Tasman Sea', *Deep-Sea Research Part I-Oceanographic Research Papers*, 53: 1989-2009.

Jeffrey, M. Z. 1986. *Climatological features of the subtropical convergence in Australian and New Zealand waters* (Ocean Sciences Institute, University of Sydney).

Kerr, Tim. 2013. 'The contribution of snowmelt to the rivers of the South Island, New Zealand', *Journal of Hydrology (New Zealand)*, 52: 61-82.

Kim, Y. S., and A. H. Orsi. 2014. 'On the Variability of Antarctic Circumpolar Current Fronts Inferred from 1992-2011 Altimetry', *Journal of Physical Oceanography*, 44: 3054-71.

Kiss, A. E., A. M. Hogg, N. Hannah, F. B. Dias, G. B. Brassington, M. A. Chamberlain, C. Chapman, P. Dobrohotoff, C. M. Domingues, E. R. Duran, M. H. England, R. Fiedler, S. M. Griffies, A. Heerdegen, P. Heil, R. M. Holmes, A. Klocker, S. J. Marsland, A. K. Morrison, J. Munroe, M. Nikurashin, P. R. Oke, G. S. Pilo, O. Richet, A. Savita, P. Spence, K. D. Stewart, M. L. Ward, F. H. Wu, and X. H. Zhang. 2020. 'ACCESS-OM2 v1.0: a global ocean-sea ice model at three resolutions', *Geoscientific Model Development*, 13: 401-42.

Kostianoy, A. G., A. I. Ginzburg, M. Frankignoulle, and B. Delille. 2004. 'Fronts in the Southern Indian Ocean as inferred from satellite sea surface temperature data', *Journal of Marine Systems*, 45: 55-73.

Mata, Mauricio M., Matthias Tomczak, Susan Wijffels, and John A. Church. 2000. 'East Australian Current volume transports at 30°S: Estimates from the World Ocean Circulation Experiment hydrographic sections PR11/P6 and the PCM3 current meter array', *Journal of Geophysical Research: Oceans*, 105: 28509--26.

Meijers, A. J. S. 2014. 'The Southern Ocean in the Coupled Model Intercomparison Project phase 5.', *Philosophical transactions. Series A, Mathematical, physical, and engineering sciences*, 372: 20130296.

Mitchell, JS, KA Mackay, HL Neil, EJ Mackay, A Pallentin, and P Notman. 2012. 'Undersea New Zealand, 1: 5,000,000. NIWA Chart', *Miscellaneous Series*.

Morris, M., B. Stanton, and H. Neil. 2001. 'Subantarctic oceanography around New Zealand: preliminary results from an ongoing survey', *New Zealand Journal of Marine and Freshwater Research*, 35: 499-519.

Oke, P. R., G. S. Pilo, K. Ridgway, A. Kiss, and T. Rykova. 2019. 'A search for the Tasman Front', *Journal of Marine Systems*, 199.

Oke, P. R., M. Roughan, P. Cetina-Heredia, G. S. Pilo, K. R. Ridgway, T. Rykova, M. R. Archer, R. C. Coleman, C. G. Kerry, C. Rocha, A. Schaeffer, and E. Vitarelli. 2019. 'Revisiting the circulation of the East Australian Current: Its path, separation, and eddy field', *Progress In Oceanography*, 176.

Oliver, E. C. J., and N. J. Holbrook. 2014. 'Extending our understanding of South Pacific gyre spin-up : Modeling the East Australian Current in a future climate', *Journal of Geophysical Research: Oceans*, 119: 2788--805.

Oliver, E. C. J., T. J. O'Kane, and N. J. Holbrook. 2015. 'Projected changes to Tasman Sea eddies in a future climate', *Journal of Geophysical Research-Oceans*, 120: 7150-65.

Orsi, A. H., T. Whitworth, and W. D. Nowlin. 1995. 'On the Meridional Extent and Fronts of the Antarctic Circumpolar Current', *Deep-Sea Research Part I-Oceanographic Research Papers*, 42: 641-73.

Ridgway, K. R., and J. R. Dunn. 2003. 'Mesoscale structure of the mean East Australian Current System and its relationship with topography', *Progress In Oceanography*, 56: 189-222.

Ridgway, Ken R., and J. R. Dunn. 2007. 'Observational evidence for a Southern Hemisphere oceanic supergyre', *Geophysical Research Letters*, 34: n/a--n/a.

Roemmich, Dean, and John Gilson. 2009. 'The 2004–2008 mean and annual cycle of temperature, salinity, and steric height in the global ocean from the Argo Program', *Progress In Oceanography*, 82: 81--100.

Roughan, Moninya, and Jason H. Middleton. 2004. 'On the East Australian Current: Variability, encroachment, and upwelling', *Journal of Geophysical Research*, 109: C07003.

Sallée, J. B., K. Speer, and R. Morrow. 2008. 'Response of the Antarctic Circumpolar Current to Atmospheric Variability', *Journal of Climate*, 21: 3020-39.

Seton, Maria, C Adams, H Campbell, Julien Collot, P King, Nick Mortimer, M Rattenbury, V Stagpoole, R Sutherland, and Andrew Tulloch. 2017. 'Zealandia: Earth's Hidden Continent'.

Sloyan, Bernadette M., Ken R. Ridgway, Rebecca Cowley, Bernadette M. Sloyan, Ken R. Ridgway, and Rebecca Cowley. 2016. 'The East Australian Current and Property Transport at 27°S from 2012 to 2013', *Journal of Physical Oceanography*, 46: 993--1008.

Smith, R. O., R. Vennell, H. C. Bostock, and M. J. M. Williams. 2013. 'Interaction of the subtropical front with topography around southern New Zealand', *Deep-Sea Research Part I-Oceanographic Research Papers*, 76: 13-26.

Smythe-Wright, D., P. Chapman, C. D. Rae, L. V. Shannon, and S. M. Boswell. 1998. 'Characteristics of the South Atlantic subtropical frontal zone between 15 degrees W and 5 degrees E', *Deep-Sea Research Part I-Oceanographic Research Papers*, 45: 167-+.

Sokolov, S., and S. R. Rintoul. 2002. 'Structure of Southern Ocean fronts at 140 degrees E', *Journal of Marine Systems*, 37: 151-84.

———. 2007. 'On the relationship between fronts of the Antarctic Circumpolar Current and surface chlorophyll concentrations in the Southern Ocean', *Journal of Geophysical Research-Oceans*, 112.

———. 2009a. 'Circumpolar structure and distribution of the Antarctic Circumpolar Current fronts: 1. Mean circumpolar paths', *Journal of Geophysical Research-Oceans*, 114: C11018.

———. 2009b. 'Circumpolar structure and distribution of the Antarctic Circumpolar Current fronts: 2. Variability and relationship to sea surface height', *Journal of Geophysical Research-Oceans*, 114: C11019.

Stanton, B. R. 2010. 'An oceanographic survey of the Tasman Front', *New Zealand Journal of Marine and Freshwater Research*, 15: 289--97.

Storkey, D., A. T. Blaker, P. Mathiot, A. Megann, Y. Aksenov, E. W. Blockley, D. Calvert, T. Graham, H. T. Hewitt, P. Hyder, T. Kuhlbrodt, J. G. L. Rae, and B. Sinha. 2018. 'UK Global Ocean GO6 and GO7: a traceable hierarchy of model resolutions', *Geoscientific Model Development*, 11: 3187-213.

Stramma, L. 1992. 'The South Indian-Ocean Current', *Journal of Physical Oceanography*, 22: 421-30.

Sutton, Philip. 2001. 'Detailed structure of the Subtropical Front over Chatham Rise, east of New Zealand', *Journal of Geophysical Research*, 106: 31045.

Sutton, Philip J. H., and Dean Roemmich. 2001. 'Ocean temperature climate off North-East New Zealand', *New Zealand Journal of Marine and Freshwater Research*, 35: 553-65.

Szymanska, K., and M. Tomczak. 1994. 'Subduction of Central Water near the Subtropical Front in the Southern Tasman Sea', *Deep-Sea Research Part I-Oceanographic Research Papers*, 41: 1373-86.

Tilburg, C. E., H. E. Hurlburt, J. J. O'Brien, and J. F. Shriver. 2002. 'Remote topographic forcing of a baroclinic western boundary current: An explanation for the Southland Current and the pathway of the subtropical front east of New Zealand', *Journal of Physical Oceanography*, 32: 3216-32.

Tsujino, Hiroyuki, Shogo Urakawa, Hideyuki Nakano, R. Justin Small, Who M. Kim, Stephen G. Yeager, Gokhan Danabasoglu, Tatsuo Suzuki, Jonathan L. Bamber, Mats Bentsen, Claus W. Böning, Alexandra Bozec, Eric P. Chassignet, Enrique Curchitser, Fabio Boeira Dias, Paul J. Durack, Stephen M. Griffies, Yayoi Harada, Mehmet Ilicak, Simon A. Josey, Chiaki Kobayashi, Shinya Kobayashi, Yoshiki Komuro, William G. Large, Julien Le Sommer, Simon J. Marsland, Simona Masina, Markus Scheinert, Hiroyuki Tomita, Maria Valdivieso, and Dai Yamazaki. 2018. 'JRA-55 based surface dataset for driving ocean–sea-ice models (JRA55-do)', *Ocean Modelling*, 130: 79-139.

Uddstrom, M. J., and N. A. Oien. 1999. 'On the use of high-resolution satellite data to describe the spatial and temporal variability of sea surface temperatures in the New Zealand region', *Journal of Geophysical Research-Oceans*, 104: 20729-51.

Williams, J., O. Morgenstern, V. Varma, E. Behrens, W. Hayek, H. Oliver, S. Dean, B. Mullan, and D. Frame. 2016. 'Development of the New Zealand Earth System Model: NZESM', *Weather and Climate*, 36: 25--44.

Yang, Hu, Gerrit Lohmann, Uta Krebs-Kanzow, Monica Ionita, Xiaoxu Shi, Dimitry Sidorenko, Xun Gong, Xueen Chen, and Evan J. Gowan. 2020. 'Poleward Shift of the Major Ocean Gyres Detected in a Warming Climate', *Geophysical Research Letters*, 47: e2019GL085868.

8. Figure and table captions

Figure 1a. Model grid sizes of the NZ20 configuration in km as colour shading. White contour line shows the 1000m iso-bath. Two sections have been defined to enclose the majority of the Tasman Sea (red dotted), the Tasman North (TN) and Tasman South (TS) section. The orange dots along the sections mark the segments which have been used to calculate transports. A meridional section at 165°E (purple dotted line) has been defined to illustrate the temperature and salinity structure over the water column in the STF region. The Macquarie Ridge (MR), Campbell Plateau (CP), Chatham Rise (CR), Bounty Through (BT), and Tasman Sea (TAS) have been labelled. (b) Schematic of major ocean currents in the region: East Australian Current (EAC), East Australian Current Extension (EAC-Ext), Tasman Front (TF), East Auckland Current (EAUC), Fiordland Current (FC), Southland Current (SC), Antarctic Circumpolar Current (ACC). The Bass Strait (BS), Cook Strait (CS), East Cape Eddy (ECE), Wairarapa Eddy (WE) and Rekohu Eddy (RE) have been labelled. The location of the Subtropical Front (STF) has been indicated by the dashed red line.

Figure 2. (a-c) Time mean SSH from AVISO, eORCA025 and NZ20 in meter for the period from 1993 to 2018. (d-f) SSH variance for AVISO, eORCA025 and NZ20 in cm^2. Contour interval is 10 cm in (a-c) and $5cm^2$ in (d-f).

Figure 3: Time averaged temperature (a) and salinity (b) profile over the Tasman Sea are presented as solid lines for Argo, eORCA025 and NZ20 for the period from 2004 to 2018. The range is shown by the colour shading.

Figure 4. Upper 200m temperature (a-b) and salt (c-d) bias of eORCA025 (left panels) and NZ20 (right panels) against Argo over the period from 2004 to 2018. The purple line (165°E) marks the section used to investigate the impact of model biases on the STF detection (Figure 7).

Figure 5. Time mean modelled temperature, salinity, cross section velocity along the Tasman North section for eORCA025 (top panels), NZ20 (middle panels) and NZ20 minus eORCA025 (bottom panels) for the period 1980 to 2018. The section starts at the Australian coast (0km) and ends at the northern tip of New Zealand (2700km). Black contour shows the 11°C/34.8 psu contour. The dashed line marks the where the zonal section turns to a meridional section.

Figure 6. Time mean modelled temperature, salinity, cross section velocity along the Tasman South section for eORCA025 (top panels), NZ20 (middle panels) and NZ20 minus eORCA025 (bottom panels) for the period 1980 to 2018. Black contour shows the 11°C/34.8 psu contour.

Figure 7. Meridional section along 165°E through the Tasman Sea. (a) Time mean (2004-2018) 11°C isotherm shown by the solid lines and ±1°C deviation by the color shading. (b) Time mean (2004-2018)

34.8 psu isohaline shown by the solid lines and ±0.2 psu deviation by the color shading. The hexagons show the location of the STF according to the isotherms and isohalines.

Figure 8. Time mean STF locations for Argo (a) and NZ20 (b) shown as solid lines for the period from 2004 to 2018. Colour shading in (a-c) shows the range in STF location with small deviation from temperature (±1 °C) and salinity (±0.2 psu) STF thresholds.

Figure 9. Seasonal meridional variation of the STF for Argo (left panels) and NZ20 (right panels) over the period 2004 to 2018. STF_{TEMP} (a, b) and STF_{SALT} (c, d). The zonal range of Australia (AUS), Tasman Sea (TAS) and Chatham Rise (CR) are shown by the respective labels on the top.

Figure 10 Interannual meridional variation of the STF for Argo (left panels) and NZ20 (right panels). over the period 1980 (2004, Argo) to 2018. STF_{TEMP} (a, b) and STF_{SALT} (c, d). The zonal range of Australia (AUS), Tasman Sea (TAS) and Chatham Rise (CR) are shown by the respective labels on the top.

Figure 11. Time series of annual integrated 0 – 500m mean (a) freshwater transport across TN and TS, (b) estimated freshwater content based on freshwater transports (color shading), true freshwater content anomaly (FWCA, S_{ref}=34.8) from NZ20 (teal) and Argo (dark blue). The color-coded dots show the meridional anomaly of the STF locations over the Tasman Sea. (c) and (d) the same diagnostic but for heat transport and heat content anomaly (HCA).

Figure 12. Correlation between integrated 0 – 500m Tasman Sea heat content proxy and SST (a), SSH (b) and wind stress curl (c) over the period from 1980 to 2018. Blue boxes mark regions for area averages for Figure 13. Hashed regions show not significant correlations.

Figure 13. Estimated 0 – 500m Tasman Sea heat content anomaly represented by the color shading. Area averaged SSH (green line, first right y-axis), SST (orange, second right y-axis) and winds stress curl (purple bars, left y axis). Regions over which the quantities have been averaged are shown in Figure 12.

Table 1. Geographic coordinates for the defined control cross sections and regions shown in Figure 1.

Table 2: Time mean model transports (1980-2018) and observational estimates for Tasman North section, Tasman South section, East Australian Current (EAC), Tasman Front, subtropical gyre (STG) and East Australian Extension.